

A New Microcontroller-Based MPPT Algorithm for Photovoltaic Applications

Ahmad Zbeeb

A Thesis
in
The Department
of
Electrical and Computer Engineering

Presented in Partial Fulfillment of the Requirements
for the Degree of Master of Applied Science (Electrical & Computer Engineering) at
Concordia University
Montréal, Québec, Canada

June 2009

© Ahmad Zbeeb, 2009



Library and Archives
Canada

Published Heritage
Branch

395 Wellington Street
Ottawa ON K1A 0N4
Canada

Bibliothèque et
Archives Canada

Direction du
Patrimoine de l'édition

395, rue Wellington
Ottawa ON K1A 0N4
Canada

Your file *Votre référence*
ISBN: 978-0-494-63080-8
Our file *Notre référence*
ISBN: 978-0-494-63080-8

NOTICE:

The author has granted a non-exclusive license allowing Library and Archives Canada to reproduce, publish, archive, preserve, conserve, communicate to the public by telecommunication or on the Internet, loan, distribute and sell theses worldwide, for commercial or non-commercial purposes, in microform, paper, electronic and/or any other formats.

The author retains copyright ownership and moral rights in this thesis. Neither the thesis nor substantial extracts from it may be printed or otherwise reproduced without the author's permission.

In compliance with the Canadian Privacy Act some supporting forms may have been removed from this thesis.

While these forms may be included in the document page count, their removal does not represent any loss of content from the thesis.

AVIS:

L'auteur a accordé une licence non exclusive permettant à la Bibliothèque et Archives Canada de reproduire, publier, archiver, sauvegarder, conserver, transmettre au public par télécommunication ou par l'Internet, prêter, distribuer et vendre des thèses partout dans le monde, à des fins commerciales ou autres, sur support microforme, papier, électronique et/ou autres formats.

L'auteur conserve la propriété du droit d'auteur et des droits moraux qui protègent cette thèse. Ni la thèse ni des extraits substantiels de celle-ci ne doivent être imprimés ou autrement reproduits sans son autorisation.

Conformément à la loi canadienne sur la protection de la vie privée, quelques formulaires secondaires ont été enlevés de cette thèse.

Bien que ces formulaires aient inclus dans la pagination, il n'y aura aucun contenu manquant.


Canada

Abstract

A New Microcontroller-Based MPPT Algorithm for Photovoltaic Applications

Ahmad Zbeeb

In this work, a new and improved microcontroller-based maximum power point tracking (MPPT) algorithm for photovoltaic (PV) applications is proposed and implemented. The algorithm incorporates new ideas for overcoming the challenges associated with rapidly changing insolation levels and the effect of partial shading. It is simple with (*i.e.* no complex computations) and can be implemented on commercial micro-controllers.

The proposed algorithm enhances the steady-state and dynamic responses by introducing an improved adaptive step-size for updating the PV module's reference variable (*i.e.* voltage, current or duty cycle). This new adaptive step-size approach exploits the first derivative of power as a function of duty cycle (dP/dD) and the sign of the second derivative for dividing the panel's operating range into four different regions. Consequently, the PV module's operating point can be tracked more precisely, thereby leading to more accurate step-size update compared to traditional step-size update.

The instability issue, under rapidly changing insolation levels, is addressed by incorporating a current measurement I_{null} at the end of each sampling period. The measured I_{null} is used to estimate power dP_2 caused by the insolation change during the sampling period, which is compared to power change dP_1 caused by MPPT update.

The algorithm also considers the issue of partial shading, where multiple peaks appear in the power function of the PV modules. The proposed algorithm exploits the

relation between the maximum power current I_{MP} and the global maximum power P_m (*i.e.* $P_m = \alpha I_{mp}$) to estimate the global maximum. Based on this relation, periodic interrupt routines are invoked to estimate the expected global maximum power P_m of the present operating current I_{pv} using ($P_m = \alpha I_{pv}$). This power P_m is then compared with the actual output power P_o to ensure that the module is operating at the global maximum.

The proposed MPPT system is modeled in SIMULINK with the theoretical models of a PV module and a buck converter. Simulation results are presented to validate the algorithm performance under different irradiation schemes, and are then compared to the results of several conventional algorithms (*e.g.* P&O, adaptive ICM). In addition, a hardware prototype is implemented where the experimental results are presented and compared to a conventional algorithm.

Acknowledgments

I would like to express my sincere appreciation to Dr. Vijay Devabhaktuni and Dr. Abdel Sebak for their tireless efforts and invaluable guidance in the advancement of my research. I am indebted to them and would like to express my great appreciation for their unfailing help and support during the course of this work.

I would also like to thank my colleagues Farzin Manouchehri, Kaustubha Mendhurwar, Navid Arbabi, and Rajasekar Kakumani for their helpful suggestions.

Finally, special thanks to my brother Haitham Zbeeb for all his help and financial support during my studies.

*To my loving parents
Hussein & Mona*

Table of Contents

LIST OF FIGURES	X
LIST OF TABLES	XIV
LIST OF SYMBOLS	XV
LIST OF ABBREVIATED TERMS.....	XVIII
CHAPTER 1. INTRODUCTION	1
1.1. INTRODUCTION TO PHOTOVOLTAIC POWER.....	1
1.2. PV CELLS CHARACTERISTICS	2
1.2.1 PV Cell Model.....	2
1.2.2 Power Characteristics.....	3
1.3. MAXIMUM POWER POINT TRACKING (MPPT).....	5
1.4. MPPT ALGORITHM.....	7
1.5. PROBLEM STATEMENT AND MOTIVATION	9
1.6. OBJECTIVES	10
1.7. THESIS ORGANIZATION	11
CHAPTER 2. LITERATURE REVIEW	12
2.1. INTRODUCTION	12
2.2. BASIC MPPT THEORY	12
2.2.1 Hill Climbing Method / Perturb and Observation.....	12
2.2.2 Incremental Conductance Method (ICM)	14
2.2.3 Open-circuit Voltage/Short-circuit Current Methods	15
2.2.4 Other Methods.....	16
2.3. APPLICATION AND IMPROVEMENT	16
2.3.1 Development of a Microcontroller-Based, Photovoltaic MPPT Control System [5]	16
2.3.2 A Modified Adaptive Hill Climbing MPPT Method for Photovoltaic Power Systems [21]...	17

2.3.3	<i>Optimization of Perturb and Observe Maximum Power Point Tracking Method [12]</i>	17
2.3.4	<i>An Intelligent Maximum Power Point Tracker Using Peak Current Control [9]</i>	18
2.3.5	<i>Constant Resistance Control of Solar Array Regulator Using Average Current [22]</i>	18
2.3.6	<i>A Method for MPPT Control While Searching for Parameters of Weather Conditions [10]</i>	19
2.3.7	<i>A Variable Step Size INC MPPT Method for PV Systems [23]</i>	19
CHAPTER 3. THE PROPOSED ALGORITHM		20
3.1.	INTRODUCTION	20
3.2.	CHARACTERISTICS OF THE PROPOSED ALGORITHM	21
3.2.1	<i>Adaptive Step-size Update</i>	21
3.2.2	<i>Rapidly Changing Atmospheric Conditions</i>	27
3.2.3	<i>Partial Shading</i>	30
3.3.	FLOW CHART	32
3.4.	CONCLUSION	34
CHAPTER 4. SIMULATION AND EXPERIMENTAL RESULTS		35
4.1.	INTRODUCTION	35
4.2.	SIMULINK SETUP	36
4.2.1	<i>Developed Model of PV Panels</i>	36
4.2.2	<i>Buck Converter Modeling</i>	40
4.2.3	<i>Complete SIMULINK Model</i>	42
4.3.	TRANSIENT /STEADY-STATE RESPONSE RESULTS AND DISCUSSIONS	44
4.3.1	<i>Comparison with P&O Algorithm</i>	46
4.4.	DYNAMIC RESPONSE RESULTS AND DISCUSSIONS	54
4.4.1	<i>First Irradiation Scheme (Comparison with Adaptive P&O)</i>	54
4.4.2	<i>Second Irradiation Scheme (Comparison with Adaptive ICM)</i>	56
4.5.	EXPERIMENTAL SETUP	59
4.5.1	<i>Overall Hardware Schematic</i>	59
4.5.2	<i>Voltage and Current Sensors</i>	61

4.5.3	<i>Buck Converter</i>	63
4.5.4	<i>Microcontroller and Interface</i>	64
4.6.	EXPERIMENTAL RESULTS	66
4.6.1	<i>Comparison with adaptive P&O</i>	68
4.7.	CONCLUSION	71
CHAPTER 5. CONCLUSIONS		72
5.1.	SUMMARY.....	72
5.2.	FUTURE WORK	75
REFERENCES		76
APPENDIX. MATLAB CODES		79

List of Figures

Figure 1.1 PV cell equivalent circuit model	2
Figure 1.2 Voltage-current characteristics of a typical PV module.....	4
Figure 1.3 Power characteristics of a typical solar module with respect to: (a) output voltage (b) output current.....	4
Figure 1.4 The effect of insolation levels on the $I-V$ characteristics of PV Panels.....	5
Figure 1.5 The effect of temperature levels on the $I-V$ characteristics of PV Panels	5
Figure 1.6 Displacement of the optimum current due to insolation variations.....	6
Figure 1.7 Displacement of the optimum voltage due to temperature variations.....	6
Figure 1.8 Introduction of an MPPT unit to a PV system	7
Figure 1.9 Typical MPPT control system.....	7
Figure 2.1 Flow chart of the hill climbing algorithm.....	13
Figure 2.2 Power-voltage characteristics of a typical PV module and its derivative	14
Figure 3.1 MPPT algorithm response with a large step-size	21
Figure 3.2 MPPT algorithm response with a small step-size.....	22
Figure 3.3 MPPT algorithm response with an adaptive step-size.....	23
Figure 3.4 Power-voltage characteristic of a typical PV module, and its derivative.....	24
Figure 3.5 Power-duty cycle characteristics of a typical PV module, and its derivative .	25
Figure 3.6 Depiction of $P-V$ curves under rapidly changing insolation levels	28
Figure 3.7 Relative changes in current and voltage due to changes in insolation levels..	29
Figure 3.8 Proposed null current measurement	29

Figure 3.9 Multiple peak in P-V curve for partially shaded modules.....	30
Figure 3.10 Relationship between maximum power P_m and corresponding maximum power current I_{mp}	31
Figure 3.11 Flow chart of the proposed algorithm	33
Figure 4.1 Modified SIMULINK model of PV modules.....	36
Figure 4.2 Modified SIMULINK model of PV modules (detailed view).....	37
Figure 4.3 Circuit model of PV cells	37
Figure 4.4 SIMULINK test system of PV modules.....	38
Figure 4.5 $I-V$ and $P-I$ characteristic of the PV model	38
Figure 4.6 P-I characteristics under different insolation levels	39
Figure 4.7 Schematic of the buck DC-to-DC converter	41
Figure 4.8 SIMULINK test system of the buck converter.....	41
Figure 4.9 Simulation results of the buck converter model.....	42
Figure 4.10 Complete SIMULINK model of the PV system.....	43
Figure 4.11 Significant outputs of the modeled PV system.....	45
Figure 4.12 Simulation results of the output voltage and output current of the PV module	46
Figure 4.13 Comparison between the proposed algorithm and P&O with step-size = 0.005	47
Figure 4.14 Error from the ideal case in (a) P&O (step-size=0.005), (b) proposed algorithm	48
Figure 4.15 Comparison between the proposed algorithm and P&O with step-size = 0.008	49

Figure 4.16 Error from the ideal case in (a) P&O (step-size=0.008), (b) proposed algorithm	49
Figure 4.17 Comparison between the proposed algorithm and P&O with step-size = 0.015	50
Figure 4.18 Error from the ideal case in (a) P&O (step-size=0.015) (b) proposed algorithm	50
Figure 4.19 Steady-state comparison between the proposed algorithm and P&O with step-size = 0.015	51
Figure 4.20 Steady-state error from the ideal case in (a) P&O (step-size=0.015) (b) proposed algorithm	51
Figure 4.21 Error comparison among the proposed algorithm and different P&O algorithms	52
Figure 4.22 Steady error comparison between the proposed algorithm and P&O (step-size=0.015).....	53
Figure 4.23 Comparison between the proposed algorithm and an adaptive P&O.....	55
Figure 4.24 Error from the ideal case in (a) adaptive P&O (b) proposed algorithm	55
Figure 4.25 Error comparison between the proposed algorithm and an adaptive P&O ...	56
Figure 4.26 Comparison between the proposed algorithm and an adaptive ICM	57
Figure 4.27 Error from the ideal case in (a) adaptive ICM (b) proposed algorithm.....	57
Figure 4.28 Error comparison between the proposed algorithm and an adaptive ICM....	58
Figure 4.29 Hardware prototype schematic	59
Figure 4.30 Kyocera 85Watt PV panel	60
Figure 4.31 Actual hardware prototype	61

Figure 4.32 Sallen & Key low pass filter.....	62
Figure 4.33 Buck converter current (a) T_{on} (b) T_{off}	63
Figure 4.34 Full hardware schematic with the microcontroller and the interface	65
Figure 4.35 Experimental output voltage of the proposed algorithm	67
Figure 4.36 Experimental output current of the proposed algorithm.....	67
Figure 4.37 Experimental output power of the proposed algorithm.....	68
Figure 4.38 Experimental output voltage of an adaptive P&O.....	68
Figure 4.39 Experimental current voltage of an adaptive P&O.....	69
Figure 4.40 Experimental output power of an adaptive P&O	69
Figure 4.41 Comparison between the proposed algorithm and an adaptive P&O.....	70
Figure 4.42 Error comparison between the proposed algorithm and an adaptive P&O ...	70

List of Tables

Table 3.1 Classification of the operating range of PV modules	26
Table 3.2 MPPT algorithms response under rapidly changing atmospheric conditions...	27
Table 4.1 Summary of the comparison cases with P&O algorithm.....	53
Table 4.2 Summary of the comparison cases with adaptive step-size algorithms.....	58
Table 4.3 PV panel specifications of the Kyocera KC85T	60
Table 4.4 Components description of the buck converter	63

List of Symbols

α	Constant relationship between I_{mp} and P_m .
β	Parameter proportional to dP_2 .
A	Ideality factor of the cell's p-n junction.
dP	Total power change between two sampling period.
dP_1	Power change due to MPPT action.
dP_2	Power change to rapid insolation changes.
E_{GO}	Band gap energy of the cell's p-n junction.
f_s	Switching frequency.
I_d	Current in the p-n junction of the PV cell.
I_g	Current generated due to photons energy.
I_{mp}	PV panel current at maximum power.
I_{null}	Introduced current at the end of the sampling period.
I_{om}	DC component of the maximum inductor current.
I_{or}	Reverse saturation current at reference temperature.
I_{pv}	Output current of the PV cell.

I_{sat}	Saturation current.
I_{sc}	Short-circuit current of the PV cell.
I_{sh}	Current in the shunt resistance of the PV cell.
K	Boltzmann's constant.
K_{N}	Scaling factor of the step-size.
N_{p}	Number of cells in parallel.
N_{s}	Number of cells in series.
P_{m}	Maximum power of the PV panel.
P_{o}	Output power of the PV panel.
q	Electron charge.
R_{s}	PV cell series resistance.
R_{sh}	PV cell shunt resistance.
T	Temperature of the PV panel.
T_{r}	Reference temperature.
V_{mp}	PV panel voltage at maximum power.
V_{oc}	Open-circuit voltage of the PV panel.
V_{om}	Maximum output voltage of the buck converter.

V_{pv}	Output voltage of the PV panel.
V_{RRM}	Maximum repetitive reverse voltage.

List of Abbreviated Terms

A/D	Analog to digital.
AM	Air mass.
CC	Constant current method.
CCVS	Current controlled voltage source.
CV	Constant voltage.
<i>I-V</i>	Current-voltage characteristics of PV panels.
ICM	Incremental conductance method.
LPF	Low pass filter.
MPP	Maximum power point.
MPPT	Maximum power point tracking.
P&O	Perturb and observation.
PV	Photovoltaic.
<i>P-D</i>	Power-duty cycle characteristics of PV panels.
<i>P-I</i>	Power-current characteristics of PV panels.
<i>P-V</i>	Power-voltage characteristics of PV panels.

Chapter 1. Introduction

1.1. Introduction to Photovoltaic Power

Renewable energy is gaining tremendous attention in both academia and industry in an effort to reduce greenhouse emissions. The main renewable sources are biomass, geothermal, hydro, photovoltaic, and wind. Photovoltaic (PV) power is expected to have the fastest annual growth rate having already shown a top growth rate of more than 50% in 2006 and 2007 [1]. PV power systems have the advantage that their installation is static (*i.e.* no moving parts), simple and quick compared to other renewable sources. Thus, they have longer lifetime span, (typically more than 20 years) [2]. Moreover, due to their low operational cost and maintenance, they provide a significant solution for powering remote areas.

Photovoltaic cells are semiconductors that have weakly bonded electrons at a level of energy called valence band [2]. When energy strikes this valence band, it frees those bonded electrons and moves them to another energy level called conduction band. At the conduction band, the electrons are able to conduct electricity through an electrical load. PV cells use the energy of photons from sunlight to break their band gap energy thereby producing DC current. Typically, PV cells produce low power (approximately 2-3 *Watts*); hence several cells are connected together to form modules and panels for higher power applications. Power regulation elements (*e.g.* battery, charge controller, converter, etc...) are also incorporated to match the output power form to the demanded application.

1.2. PV Cells Characteristics

1.2.1 PV Cell Model

The equivalent circuit model of PV cells is shown Fig.1.1 [3], where we notice four traversing currents I_g , I_d , I_{sh} , and I_{pv} . Applying KCL to the circuit will lead to

$$I_{pv} = I_g - I_d - I_{sh}. \quad (1.1)$$

By substituting I_d and I_{sh} with their equivalent functions, we obtain the characteristic equation of PV panels [3],

$$I_{pv} = N_p I_g - N_p I_{sat} \left(\exp \left[\frac{q}{N_s A k T} (V_{pv} + I_{pv} R_s) \right] - 1 \right) - \frac{V_{pv} + I_{pv} R_s}{R_{sh}}, \quad (1.2)$$

where N_s and N_p are the number of cells connected in series and parallel respectively, I_g is the current generated by photons energy, I_{sat} is the reverse saturation current, q is the electron charge, A is the ideality factor, K ($eV.k^{-1}$) is the Boltzmann's constant, T (Kelvin) is the cell temperature, R_s and R_{sh} are the cell's series resistance and shunt resistance respectively, I_{pv} and V_{pv} are the cell's output current and voltage respectively.

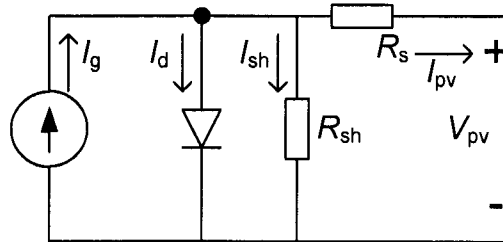


Figure 1.1 PV cell equivalent circuit model

The saturation current is defined as [2][3]

$$I_{\text{sat}} = I_{\text{or}} \left[\frac{T}{T_r} \right]^3 \exp \left[\frac{qE_{\text{GO}}}{kA} \left(\frac{1}{T_r} - \frac{1}{T} \right) \right], \quad (1.3)$$

where I_{or} is the reverse saturation current at reference temperature, T_r (Kelvin) is the reference temperature, and E_{GO} (e.V) is the band gap energy.

Finally, the current generated due to photons energy is defined as [2][3],

$$I_{\text{g}} = [I_{\text{sc}} + k_i(T - T_r)] \frac{\lambda}{100}, \quad (1.4)$$

where I_{sc} is the short circuit current at standard test conditions, k_i ($A^\circ C$) is the short circuit current temperature coefficient, and λ (mW/m^2) is the insolation level.

Standard test condition, also defined as an Air Mass 1.5 (AM1.5), implies an illumination intensity of $1000W/m^2$ striking the solar panel and a temperature of $25^\circ C$ [2][4]. The Air Mass is a measure of how the atmosphere affect the spectral distribution and intensity of the light illuminated. AM1.5 is the air mass of pure air taking into consideration the humidity and pollution of an average bright day [3].

1.2.2 Power Characteristics

The operating voltage V_{pv} and operating current I_{pv} are very critical in order to exploit the maximum efficiency of PV modules. Using (1.2)-(1.4), we can study the behaviour of the voltage as a function the current (*i.e.* current-voltage characteristics) of a typical PV module under standard test conditions. This current-voltage (I - V) characteristics is shown in Fig.1.2, where the voltage is limited by the open-circuit voltage V_{oc} and the current is limited by the short-circuit current I_{sc} . Using this I - V

relation, the output power (P_o) can be analyzed with respect to the output voltage V_{pv} and the output current I_{pv} , where $P_o = V_{pv} \times I_{pv}$. For this purpose, P_o versus V_{pv} and P_o versus I_{pv} are plotted in Fig.1.3 (a) and Fig.1.3 (b), respectively. From these plots, we notice a unique optimum voltage V_{mp} and optimum current I_{mp} corresponding to the maximum power output. Consequently, operating PV modules at their maximum efficiency implies the operation at the optimum point (*i.e.* V_{mp} and I_{mp}).

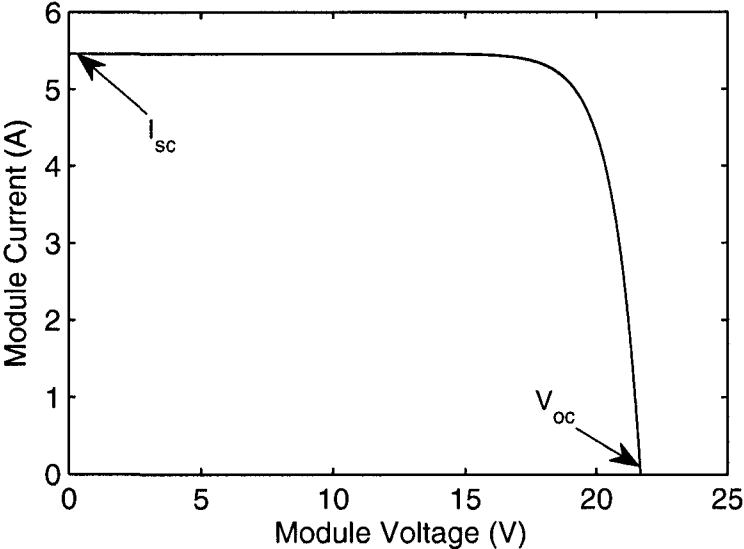


Figure 1.2 Voltage-current characteristics of a typical PV module

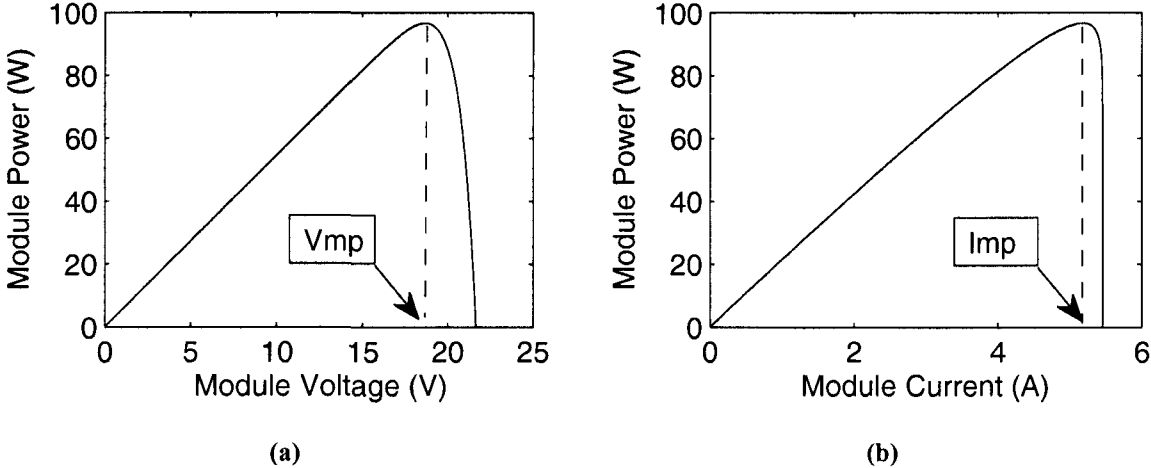


Figure 1.3 Power characteristics of a typical solar module with respect to: (a) output voltage (b) output current

1.3. Maximum Power Point Tracking (MPPT)

The $I-V$ characteristics of PV panels are altered with the variation of atmospheric conditions (*i.e.* insolation and temperature). Simulation results show the $I-V$ curve deviation due to variations in insolation levels (Fig.1.4) and temperature levels (Fig.1.5).

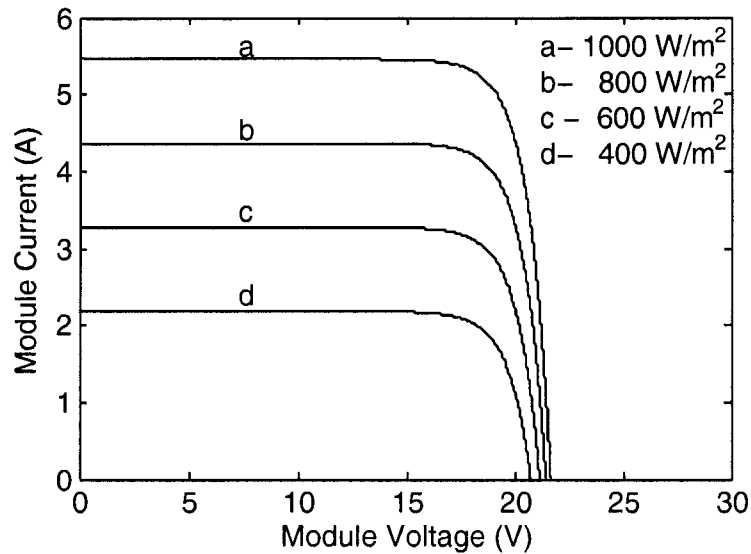


Figure 1.4 The effect of insolation levels on the $I-V$ characteristics of PV Panels

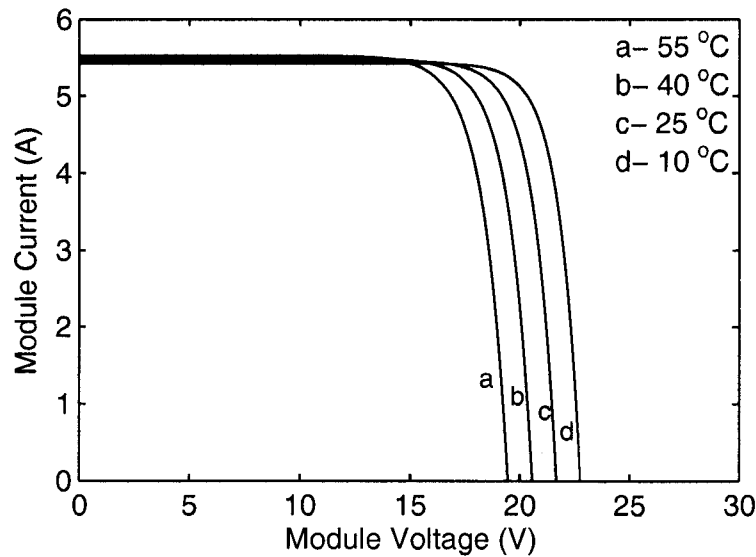


Figure 1.5 The effect of temperature levels on the $I-V$ characteristics of PV Panels

This change in the I - V characteristics leads to the displacement of the optimum current I_{mp} as shown in Fig.1.6, and the optimum voltage V_{mp} as shown in Fig.1.7. Note that I_{mp} is mainly affected by the insolation levels; whereas, V_{mp} is affected by temperature levels. As a result, the maximum power point tracking (MPPT) concept was introduced to track I_{mp} and V_{mp} under those varying atmospheric conditions [3].

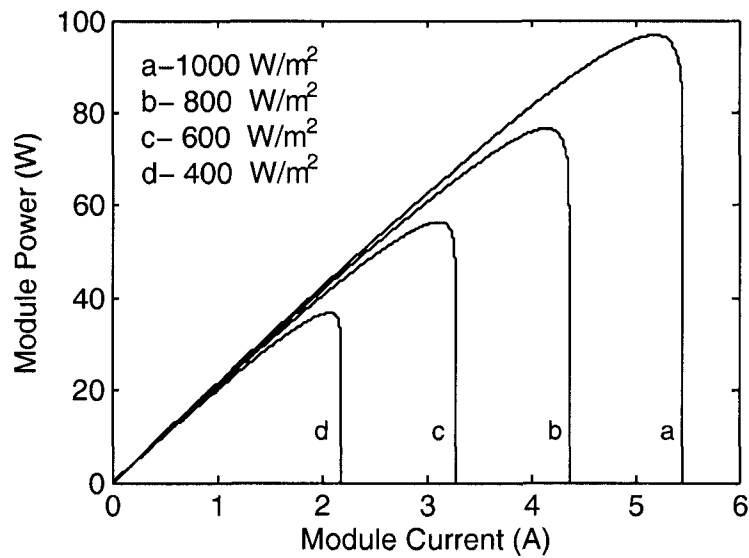


Figure 1.6 The effect of insolation levels on the P - I characteristics of PV Panels

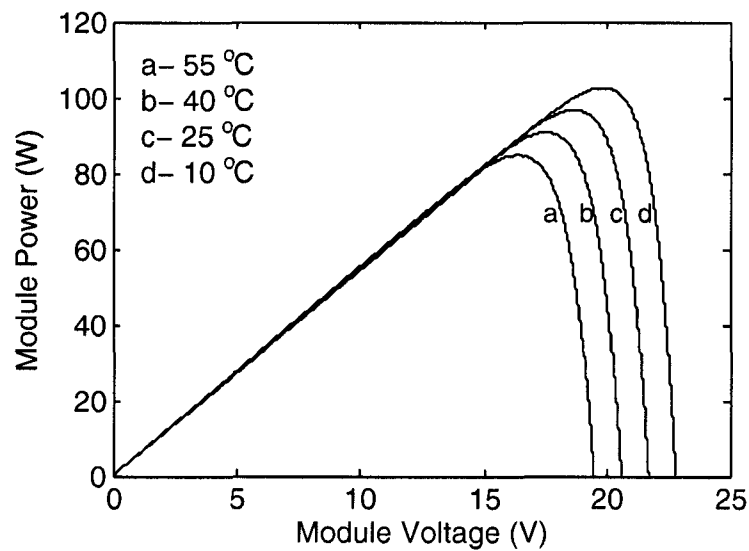


Figure 1.7 The effect of temperature levels on the P - V characteristics of PV Panels

The MPPT is achieved by introducing a DC-to-DC converter between the PV module and the load as shown in Fig.1.8 [3][5]. This DC-to-DC converter, by changing its duty cycle, can match the impedance of the source (*i.e.* PV module) to that of the load for maximum power transfer. In conclusion, MPPT units aim to dynamically move the module's operating point (*i.e.* I_{pv} , V_{pv}) to the optimum point (I_{mp} , V_{mp}) under varying insolation and temperature levels.

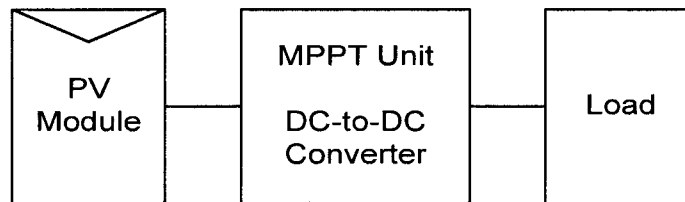


Figure 1.8 Introduction of an MPPT unit to a PV system

1.4. MPPT Algorithm

As mentioned earlier, the goal of MPPT algorithms is to move the operating point of PV module's to the optimum point (I_{mp} , V_{mp}). This is done by continuously altering the duty cycle of the DC-to-DC converter. Some MPPT controllers use analog circuitry to update the duty-cycle while the majority use digital ones. The typical and basic control system of MPPT controllers is shown in Fig.1.9 [5].

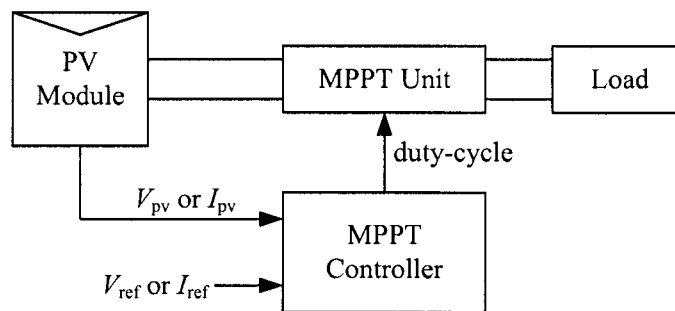


Figure 1.9 Typical MPPT control system

Different MPPT algorithms use different methods to periodically predict a reference voltage V_{ref} or reference current I_{ref} close as much as possible to the optimum point (V_{mp} , I_{mp}). Consequently, we can distinguish between two control methods used by MPPT algorithms to change the operating point of the PV panel.

1- *Voltage feedback control*: These algorithms assume a value for the optimum voltage V_{mp} in each sampling period and set it as a reference voltage (V_{ref}). Afterwards, they start altering the duty cycle of the converter till the panel's voltage V_{pv} reaches the reference voltage [5]-[8].

2- *Current feedback control*: Similar to voltage feedback control, these algorithms assume a value for the optimum current I_{mp} in each sampling period and set it as a reference current I_{ref} . Afterwards, these algorithms start altering the duty cycle of the converter till the panel's current I_{pv} reaches the reference current [9]-[11].

In addition, some algorithms directly use the duty-cycle as the control variable rather than a voltage or a current reference [12]-[14]. The most commonly used MPPT algorithms are the hill climbing method and the incremental conductance method which are briefly introduced below and explained in details in chapter 2.

Hill Climbing: This concept uses trial-and-error approach in the sense that it perturbs the solar array's reference variable, e.g. voltage, in each sampling period along a trial direction. In the next cycle, the output power is calculated to check if the power gradient is positive; otherwise, the perturbation direction is reversed [3][5][6][9][12].

Incremental Conductance Method (ICM): This method is based on the fact that the derivative of the power with respect to voltage (dP/dV) is equal to zero at the maximum

power point. Consequently, this method calculates dP/dV and update the control variable along the direction of increasing power (*i.e.* where dP/dV tend to zero) [8][10][13].

1.5. Problem Statement and Motivation

Several MPPT algorithms have been proposed throughout the literature; however, most of those algorithms have certain disadvantages. While some algorithms have drawbacks such as instability, steady-state power oscillation, etc; algorithms that address those challenges suffer from larger sampling times and increased hardware costs.

Listed below is a summary of the main factors that an efficient MPPT algorithm should take into consideration.

- *Dynamic response*: It is the speed of continuously tracking the maximum power point. An algorithm with a fast dynamic response can considerably increase the output power.
- *Steady state response*: After the maximum power point is reached, it is imperative to minimize the oscillation around this point thus minimizing power losses.
- *Rapidly changing atmospheric conditions*: In the case of rapidly changing atmospheric conditions (*e.g.* cloudy day), MPPT algorithms can be unstable and track in a wrong direction.
- *Partial shading*: Many MPPT algorithms do not consider the effect of partial shading where multiple peaks appears in the power function. Consequently, such algorithms get trapped in a local maximum (not the global maximum), and deliver a lower peak power.
- *Simplicity*: The simplicity of MPPT algorithms is essential to have short sampling periods (*i.e.* faster tracking).

Motivated by the above concerns, this work focuses on formulation of a new MPPT algorithm that is simple yet robust. The algorithm will take into account all the challenges and concerns that are presented throughout the literature (*e.g.* rapidly changing atmospheric conditions, partial shading, etc). Furthermore, considerable efforts will be focused on making the algorithm suitable to be implemented on commercial microcontrollers. This is in an attempt to fabricate cheap and efficient MPPT units, thus promoting the use of PV power on the domestic scale.

1.6. Objectives

The main objectives of this work can be summarized as follows:

- Propose a new MPPT algorithm which is based on the power-duty-cycle characteristics of buck converters. Owing to its simplicity, the algorithm is suitable to be implemented on low-architecture microcontrollers.
- The proposed algorithm should incorporate a new rule for updating the adaptive step-size of the reference variable. Moreover it is characterized by microcontroller-compatible techniques to overcome the issues of rapidly changing atmospheric conditions and partial shading.
- Implementation of a PV system on SIMULINK to test the proposed algorithm and compare its response to various algorithms.
- Implementation a hardware prototype utilizing a buck converter and a microcontroller.

1.7. Thesis organization

Chapter 1 has presented a detailed analysis of the practical model of PV panels and their I - V characteristics. It has also outlined the need for MPPT units and spotted the lights on the main concepts of MPPT algorithms. This was followed by the problem statement and motivation of this work.

Chapter 2 first analyzes in details the main concepts used in formulating MPPT algorithms. Afterwards, a literature review on selected works in this field is presented. These selected works are based on different MPPT concepts and cover the main enhancements done in this field.

Chapter 3 presents the proposed algorithm and details the techniques used to improve its efficiency especially under unstable weather conditions. It starts by introducing a new rule for updating the step-size in MPPT algorithms. Then, it describes the methods used to overcome the problems of rapidly changing atmospheric conditions and partial shading. This chapter is concluded by the flow chart of the complete algorithm.

Chapter 4 describes the SIMULINK model of the complete PV system with an emphasis on the modified model of PV panels. The experimental setup is also described in this chapter along with all related issues of hardware design and implementation. Finally it presents the experimental and simulation results showing the improvements under different irradiation schemes in comparison to different conventional algorithms.

Chapter 5 summarizes this work and the results obtained. It also highlights the possibility of any future work.

Chapter 2. Literature Review

2.1. Introduction

In this chapter, the basic concepts of MPPT algorithms will be analyzed; these concepts will include the Perturb and Observation (P&O), the Incremental Conductance Method (ICM), the open-circuit voltage/short-circuit current method, and an overview on other concepts. In the following section, a review on selected works on MPPT algorithms will be presented. These selected works will almost cover all the enhancements done in this field.

2.2. Basic MPPT Theory

2.2.1 Hill Climbing Method / Perturb and Observation

This method, also known as Perturb and Observation (P&O), perturbs the reference variable (*i.e.* voltage, current or duty cycle) using a trial and error approach to get closer to the optimum point [3][5][6][9][12].

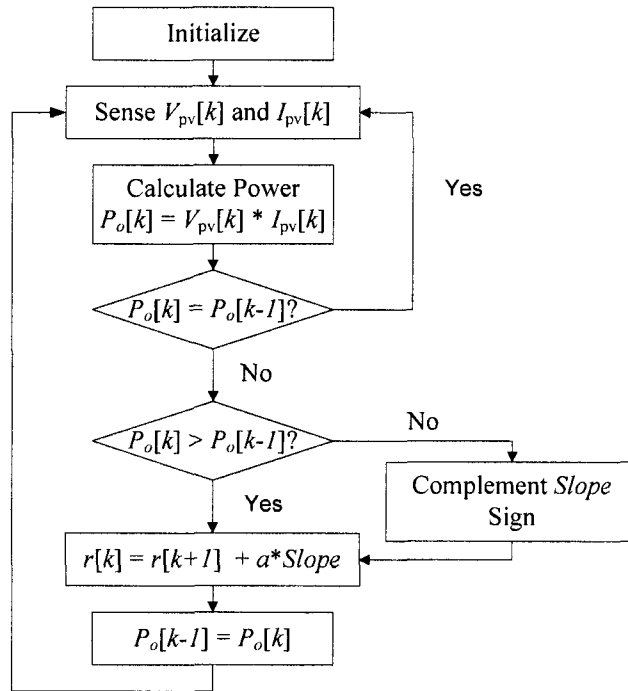


Figure 2.1 Flow-chart of the hill climbing algorithm

The flow chart of this algorithm is shown in Fig.2.1; this algorithm periodically changes the reference variable $r[k]$ by a fixed step-size (a) along the direction of increasing power. First, the panel's output voltage $V_{pv}[k]$, and output current $I_{pv}[k]$ are sensed to calculate the output power $P_o[k]$. This power is then compared to the previously calculated power $P_o[k-1]$, and the perturbation direction of the reference variable is reversed if $P_o[k] < P_o[k-1]$ (*i.e.* the tracking direction is not toward the maximum power point).

What characterizes this method is its simplicity and speed where no complex calculations are involved. However, it mainly suffers from steady state power oscillations as it continues perturbing the reference variable even when the steady state is reached.

2.2.2 Incremental Conductance Method (ICM)

This method, also known as perturb and observation method (P&O), calculates the derivative of the output power with respect to voltage (dP/dV) to predict the direction of the reference variable update [8][10][13][15].

The power-voltage ($P-V$) characteristics of PV modules and its derivative dP/dV are shown in Fig.2.2. It is noticed that the function dP/dV is positive to the left of the maximum power point (MPP), negative to the right side of the MPP, and zero at the MPP. Consequently, this algorithm periodically calculates dP/dV using Eq. (2.1) [15],

$$\frac{dP}{dV} = \frac{d(I * V)}{dV} = V_{pv}[k] * \frac{I_{pv}[k] - I_{pv}[k-1]}{V_{pv}[k] - V_{pv}[k-1]} + I_{pv}[k], \quad (2.1)$$

Finally the reference variable (*e.g.* voltage) is moved to the right (if $dP/dV > 0$), to the left (if $dP/dV < 0$), or held constant if ($dP/dV = 0$).

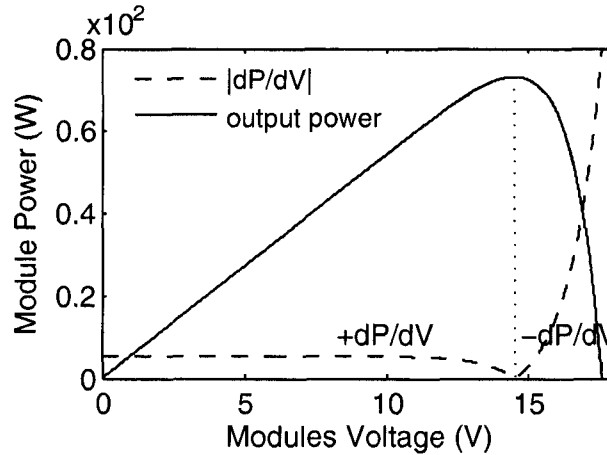


Figure 2.2 Power-voltage characteristics of a typical PV module and its derivative

This method has two advantages over the P&O method especially that it stops updating the reference variable when the MPP is reached, thus reducing power oscillations. Also, it calculates the correct direction to update the reference variable, rather than the trial and error approach. A disadvantage of this method (ICM) is that it is slower than the P&O due to extra and more complex arithmetic computations.

2.2.3 Open-circuit Voltage/Short-circuit Current Methods

The open-circuit method, also referred to as the constant voltage (CV) method, is based on the fact that the magnitude of the maximum power voltage V_{mp} is approximately 76% of the open-circuit voltage V_{oc} . Consequently, the PV module is periodically disconnected from MPPT unit to measure the open-circuit voltage V_{oc} , and the reference voltage is set to $0.76 * V_{oc}$ [16].

Similar to the open-circuit voltage method, the short-circuit current method, also referred to as the constant current (CC) method, is based on the fact that the magnitude of the maximum power current I_{mp} is approximately 90% of the short-circuit current I_{sc} . Consequently, the PV module is periodically disconnected from MPPT unit to measure the short-circuit current I_{sc} , and the reference voltage is set to $0.9 * I_{sc}$.

These methods have the advantage of simplicity as only one multiplication is needed to set the reference voltage or current. A striking disadvantage of the CV and CC methods is that PV modules need to be periodically disconnected from the MPPT for a very short time (to measure V_{oc} and I_{sc}). This results in considerable power losses on the long run; in addition to increased hardware complexity.

2.2.4 Other Methods

The main other MPPT algorithms can be summarized by the parasitic capacitance method, and the non-linear methods. The parasitic capacitance method, which is derived from the ICM, takes into consideration the average ripple of the module voltage to perturb the array's reference variable.

Non-linear methods such fuzzy logic [17][18] and neural network methods [19][20] have been presented in the literature. These methods focus on the non-linear characteristics of PV modules; however, they lack the adaptability required especially when upgrading the existing PV systems, and involve rigorous computations

2.3. Application and Improvement

2.3.1 Development of a Microcontroller-Based, Photovoltaic MPPT Control System [5]

The authors in this work present a complete analysis of a microcontroller-based MPPT system. The algorithm used is the Perturb and Observation (P&O), and the control variable chosen is the duty-cycle. This MPPT system is completely driven by a microcontroller utilizing A/D modules to read the panel's voltage and current, and a Pulse Width Modulation (PWM) module to control the duty cycle of the converter. The microcontroller periodically senses the panel's voltage and current to calculate the power $P[k]$ and compare it with power $P[k-1]$ measured during the previous sampling instant. Finally, if $P[k] < P[k-1]$ (*i.e.* power is decreasing) the perturbation direction of the duty-cycle is reversed through the PWM module.

2.3.2 A Modified Adaptive Hill Climbing MPPT Method for Photovoltaic Power Systems [21]

This work proposed an adaptive step size to update the reference variable (duty-cycle) of the traditional Hill Climbing method. The adaptive step-size $a[k]$ is periodically updated in proportion with the power difference between the last two consecutive sampling instants (*i.e.* $a[k] = M * \Delta P$, where M is a constant). This leads to large step size when the operating point is distant from the optimum point and to a small step size when the operating point is in the close vicinity of the optimum point. The proposed algorithm also incorporates an online tuning of different parameters of the hill climbing method. This approach ensures a faster dynamic response and a more stable steady-state response.

2.3.3 Optimization of Perturb and Observe Maximum Power Point Tracking Method [12]

A theoretical analysis has been presented on the choice of the parameters of the P&O algorithm. This customization of the P&O parameters is dependent on the topology of the DC-to-DC converter adopted (e.g. buck topology, boost topology, etc...) in a given MPPT system. This is in an effort to improve the dynamic response of the P&O algorithm for a specific converter's topology. An example has been provided on the boost converter, and simulation and experimental results were presented to show the efficiency of the MPPT system after the customization of the parameters.

2.3.4 An Intelligent Maximum Power Point Tracker Using Peak Current Control

[9]

A new algorithm is proposed which is derived from the Perturb and Observation (P&O) method. This algorithm exploits the simplicity and speed of the P&O and improves it by utilizing fuzzy logic based control. In addition, the principle of peak current control is adopted; this principle uses the instantaneous value of the current rather than the average value. Consequently, the current reference is constantly adjusted in accordance with the variation of the output current and voltage of the PV module. Simulation results of the proposed algorithm are presented under different irradiation schemes and compared to the fixed current reference algorithm where the transient and steady-state improvements are highlighted.

2.3.5 Constant Resistance Control of Solar Array Regulator Using Average Current [22]

The main idea behind this work is to use one control current control loop to accomplish both the MPPT action and the battery charging control. The concept of the constant resistance method is to dynamically change the effective resistance of the load into a constant resistance to always ensure the stability of the MPPT system. This concept is then modified when the load used is a battery rather than a constant resistive load. The small signal analysis is carried out to analyze the parameters of this algorithm and ensure its stability. A hardware setup has been implemented using 180Watts PV panel; the experimental results verify the system's stability over the entire region of the solar array.

2.3.6 A Method for MPPT Control While Searching for Parameters of Weather Conditions [10]

A completely new concept for MPPT algorithms is presented by the authors of this work. This proposed algorithm studies and focuses on the linearity between the maximum power (P_M) and the maximum power current (I_{MP}) under different weather conditions. Exploiting this linearity, a prediction line is formed to track the maximum power point. Consequently, the operating point is analyzed with respect to this prediction line (*i.e.* above or below), and the direction of the reference variable is determined afterwards. A hardware prototype of a PV system was implemented where the results showed a significant improve in the dynamic response.

2.3.7 A Variable Step Size INC MPPT Method for PV Systems [23]

This work has presented an advanced incremental conductance method (ICM) with a variable step-size. The proposed algorithm uses the traditional ICM to exploit its robustness, and improves it by an adaptive step-size to improve the transient and steady-state responses. The authors have presented a complete theoretical analysis of the proposed algorithm along with the design principles. The algorithm is simple and can be easily implemented in digital signal processors. Simulation and experimental results were presented; however, the results were only compared to algorithms with fixed step-sizes.

Chapter 3. The Proposed Algorithm

3.1. Introduction

The proposed algorithm focuses on improving tracking speed and stability, as well as overcoming the effects of partial shading and rapidly changing weather conditions. Owing to its simplicity, the proposed control method is suitable for implementation on commercially available micro-controllers. Further, it is cost-effective, as it makes use of hardware modules (A/D, interrupt service routines, etc) that come with such micro-controllers.

The reference variable chosen in the proposed algorithm is the duty-cycle, and a new rule is presented for its update. This rule is inherited from the conventional adaptive step-size rule, and is further modified for better tracking. The power converter chosen is the buck DC-to-DC converter, and the design formulas are based on the characteristics of this specific converter.

3.2. Characteristics of the Proposed Algorithm

3.2.1 Adaptive Step-size Update

Choosing the step-size in MPPT algorithms has always been very critical since it can considerably affect the overall performance of the algorithm. As can be seen in Fig.3.1, a large step-size leads to a better transient response (*i.e.* faster tracking), but results in large power oscillations in the steady-state. On the other hand, the choice of a small step-size leads to a slower transient response but less power oscillation at the steady state (see Fig.3.2). Consequently, the selection criterion of the step-size is contingent on the best trade-off between the transient response speed and the steady-state oscillation.

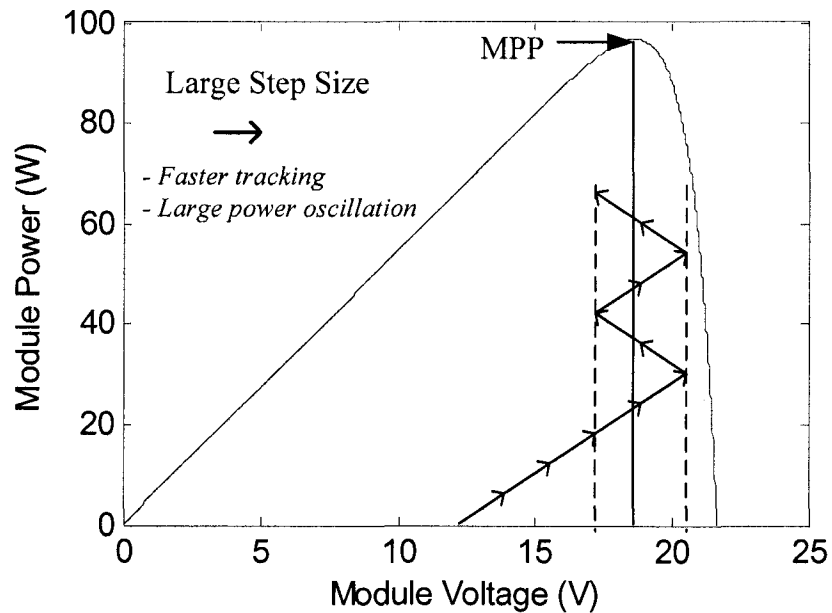


Figure 3.1 MPPT algorithm response with a large step-size

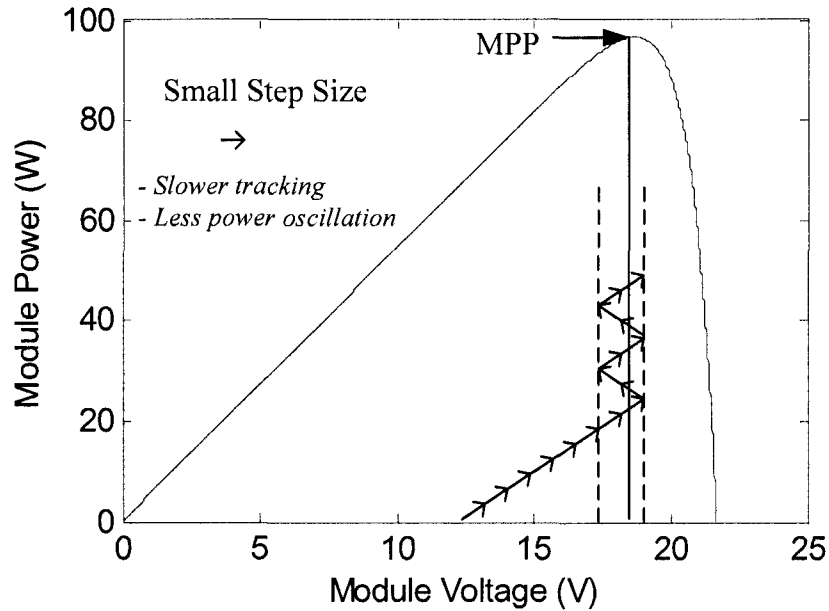


Figure 3.2 MPPT algorithm response with a small step-size

In an effort to resolve the ambiguity of choosing the proper step-size value, the principle of adaptive step-size was introduced [6][8][21][23]-[25]. This principle adjusts the step-size value according to the position of the operating point. Thus, a large step-size value is set when the operating point is away from the maximum power point (MPP) and vice-verse. Consequently, this assures a fast transient response, in addition to small power oscillations at the steady state. The adaptive step-size principle is illustrated in Fig.3.3.

However, the adaptive step-size principle requires locating the position of the operating point (*i.e.* position with respect to the MPP) to estimate the new step-size value.

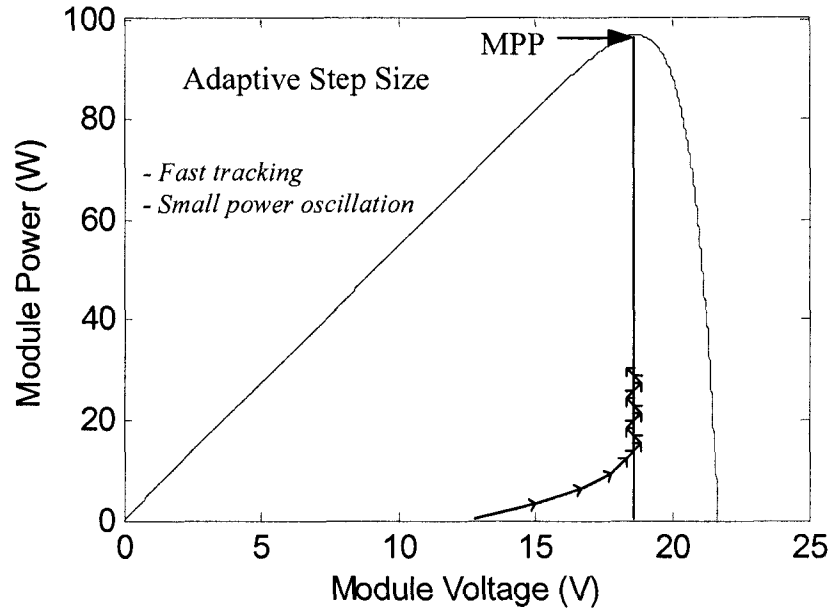


Figure 3.3 MPPT algorithm response with an adaptive step-size

In the literature, several methods have adopted the adaptive step-size principle in MPPT algorithms [6][8][21][23]-[25]. These methods typically use the first derivative of power as a function of voltage, *i.e.* dP/dV , for locating the position of the operating point, and then estimate the step size. To further elaborate, we plot in Fig.3.4 the power-voltage function (P - V) of a typical PV module along with its derivative (*i.e.* $|dP/dV|$). As can be noted, $|dP/dV|$ decreases as we approach the MPP from the left or right side, and it reaches zero at the MPP. Hence, the value of dP/dV can be used to estimate the position of the operating point with respect to the MPP. Consequently, the reference variable is updated using a variable step size, *i.e.*

$$r(k) = r(k-1) \pm a(k), \quad (3.1)$$

where $r(k)$ is the new/updated reference variable, $r(k-1)$ is its present value, $a(k)$ is the variable step size which is defined as [21][23],

$$a(k) = K_N \left| \frac{dP}{dV} \right|, \quad (3.2)$$

where K_N is a scaling parameter.

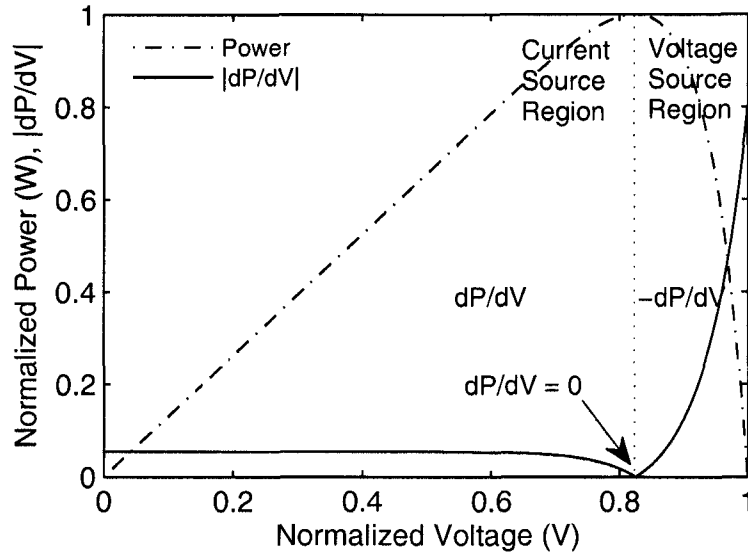


Figure 3.4 Power-voltage characteristic of a typical PV module, and its derivative

Analyzing the formula of the step-size update, one can notice that the value of $a(k)$ decreases as the operating point approaches the MPP. However, the function dP/dV , e.g. Fig.3.4, is relatively flat in the current source region and varies dramatically in the voltage source region [13]. Consequently, estimating the step size can be tough in the current source region, except when the module operates in the close vicinity of the optimum point. Dramatic variations of dP/dV in the voltage source region make it difficult to establish a universal scaling factor K_N , which can adapt to (i) a large insolation range and/or (ii) PV system upgrades, e.g. addition of PV panels [13].

In the proposed algorithm, a modified rule for updating the reference variable, *i.e.* current/voltage/duty-cycle, is presented. The rule is based on both first and second derivatives of power as a function of duty cycle (P - D) shown in Fig 3.5.

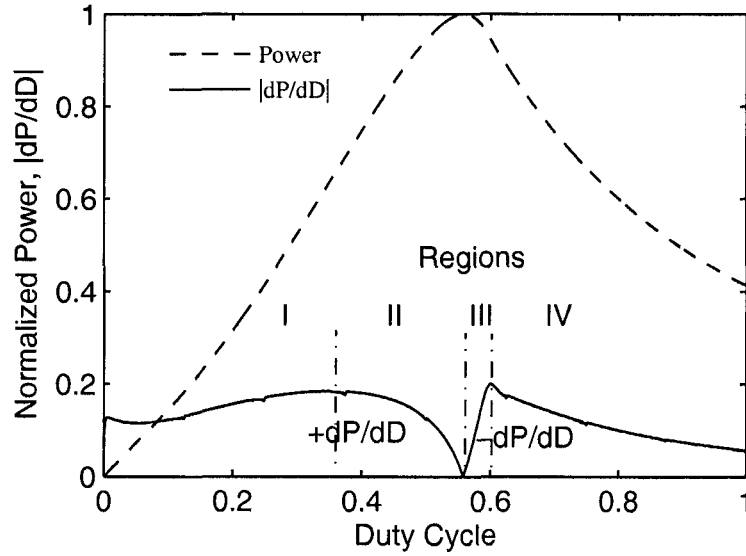


Figure 3.5 Power-duty cycle characteristics of a typical PV module, and its derivative

Unlike dP/dV , the first derivative of the P - D characteristic is non-monotonic. Based on this observation, we advocate using the sign of its second derivative, *i.e.*

$$\Delta \frac{dP}{dD} = \left(\frac{dP}{dD} \right)_k - \left(\frac{dP}{dD} \right)_{k-1}, \quad (3.3)$$

for guiding the MPPT algorithm. The sign of $\Delta(dP/dD)$ defined in (3.3) allows us to discern the overall operating range into four different regions as shown in Fig. 2. The regions classification is outlined in Table 3.1.

Table 3.1 Classification of the operating range of PV modules

Region	dP/dD	$\Delta(dP/dD)$
I	+ve	+ve
II	+ve	-ve
III	-ve	-ve
IV	-ve	+ve

Based on this new idea, we propose a new rule to update the reference variable,

$$r(k) = \begin{cases} r(k-1) + \left(D_{\max} - K_N \left| \frac{dP}{dD} \right| \right) & \text{Region I} \\ r(k-1) + K_N \left| \frac{dP}{dD} \right| & \text{Region II} \\ r(k-1) - K_N \left| \frac{dP}{dD} \right| & \text{Region III} \\ r(k-1) - \left(D_{\max} - K_N \left| \frac{dP}{dD} \right| \right) & \text{Region IV} \end{cases}, \quad (3.4)$$

where D_{\max} is the maximum allowed step size (user-defined and PV system specific).

Further elaboration of the above rule, one can see that in regions I and IV dP/dD is increasing towards the MPP (Fig.3.5), whereas it is decreasing in regions II and III towards the MPP. Consequently, in regions I and IV the step-size $D_{\max} - K_N * |dP/dD|$ decreases as we approach the MPP and increases as we move away from it; similarly for the step size in regions II and III (*i.e.* $K_N * |dP/dD|$). Using this approach, the PV module's operating point can be identified more precisely and in a wider range, thereby leading to an accurate step-size update.

The main advantage of this new adaptive step-size update is that it is practical for implementation on low-architecture micro-controllers. This is due to the fact that there are neither constant behaviour nor dramatic variation in the dP/dD curve in contrast to the traditional approach that uses dP/dV or dP/dI .

3.2.2 Rapidly Changing Atmospheric Conditions

When insolation levels change rapidly, *e.g.* on a partially cloudy day, MPPT algorithms can track in wrong directions, due to fast/large power fluctuations. These fast power changes can be misleading since they occur within the sampling period, and are confused with power change due to MPPT action [21][26][27]. To further explain the MPPT response under rapidly changing atmospheric condition, the following terms are defined,

dP : The actual power change which consists of dP_1 and dP_2 .

dP_1 : The power change due to MPPT action.

dP_2 : The power change due to fast/large power fluctuations during the sampling period.

The confusion in tracking happens if and only if the fast/large power fluctuations (dP_2) are greater than power changes (dP_1) due to MPPT update [26]. The four possible cases of the current tracking state, and the state read by the MPPT algorithm is shown in the table below,

Table 3.2 MPPT algorithms response under rapidly changing atmospheric conditions

MPPT Direction	$dP_2 > dP_1?$	Direction read by MPPT algorithm
Correct	Yes	Wrong
Correct	No	Correct
Wrong	Yes	Correct
Wrong	No	Wrong

An example is illustrated in Fig. 3.6, where a wrong update by the MPPT from point *A* to *B* can appear/seem to be a correct update, if the insolation increases suddenly to 600 W/m^2 during the sampling period. As a result, these wrong readings can cause tracking in wrong direction in the next cycle or even instability for some algorithms.

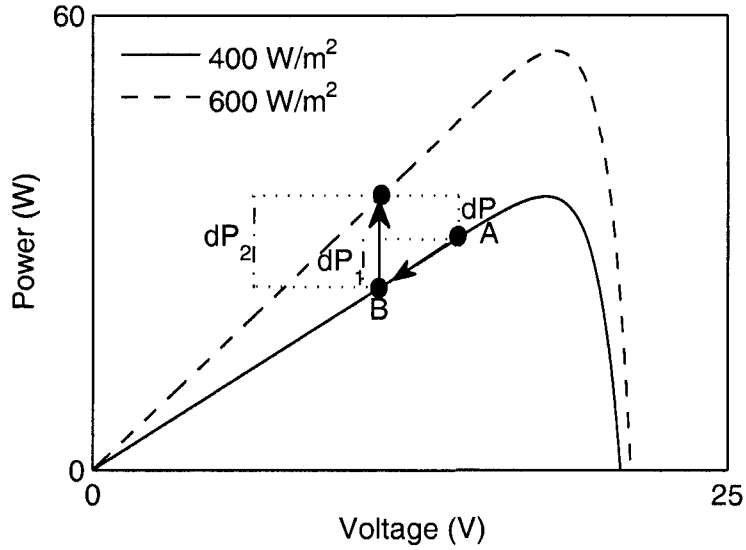


Figure 3.6 Depiction of P - V curves under rapidly changing insolation levels

The proposed algorithm addresses this issue by introducing a new technique, which separates the actual power change dP into components dP_1 and dP_2 . As mentioned, dP_2 results from fast insolation changes; insolation changes mainly affect the output current I_{PV} of the PV module rather than the output voltage V_{pv} . This fact can be seen by the simulation results of Fig. 3.7. Exploiting this property, we can use the change of current within the sampling period to estimate the dP_2 . Knowing that MPPT algorithms are able to read the actual power change dP ; then, once dP_2 is approximated, the other component dP_1 can be computed.

The component, dP_2 can be estimated by introducing a null current measurement I_{null} of the PV module at the end of each sampling period (see Fig. 3.8). We define a new parameter

$$\beta_k = I_{null} - I_k. \quad (3.5)$$

This parameter β is proportional to power changes due to insolation levels during the sampling period (*i.e.* independent of the MPPT update). This parameter is first used to estimate dP_2 , using Eq. (3.6), and dP_1 can be calculated using Eq. (3.7).

$$(dP_2)_k = V_k \beta_k. \quad (3.6)$$

$$(dP_1)_k = (dP)_k - (dP_2)_k. \quad (3.7)$$

In terms of the MPPT action, the subsequent reference variable update is reversed if $|dP_2| > |dP_1|$.

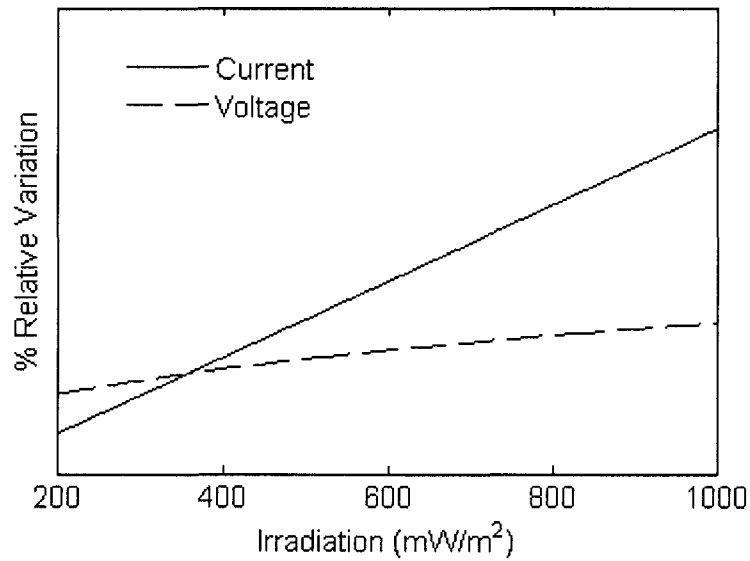


Figure 3.7 Relative changes in current and voltage due to changes in insolation levels

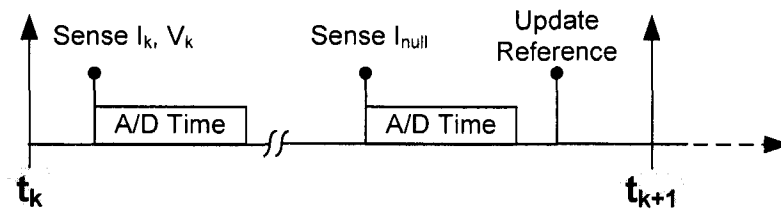


Figure 3.8 Proposed null current measurement

In summary, this strategy can considerably overcome the effect of rapidly changing atmospheric conditions in MPPT algorithm. The introduction of the null current at the end of each sampling can detect the power change dP_2 within the complete sampling period except for the intervals of A/D time (see Fig.3.8). However, these time intervals are negligible in state of the art microcontrollers (*i.e.* approx. A/D time: 19 μ s).

3.2.3 Partial Shading

Typical MPPT algorithms do not consider the effect of partial shading, *e.g.* multiple peaks in the power function as shown in Fig.3.9 [28][29]. Consequently, such algorithms get trapped in a local maximum (not the global maximum), and deliver a lower peak power. Some existing algorithms periodically scan the P - V curve, while others advocate periodic sensing of either short-circuit current I_{sc} or open-circuit voltage V_{oc} , for moving closer to the optimum reference variable. However, such methods could lead to power losses, *e.g.* those caused by disconnection of the PV array while measuring I_{sc} or V_{oc} [26].

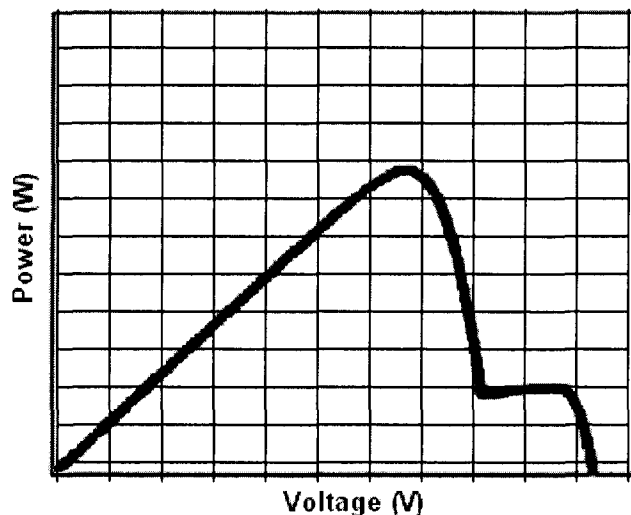


Figure 3.9 Multiple peak in P-V curve for partially shaded modules

In the proposed algorithm, we exploit the constant relation, *i.e.* $\alpha = I_{mp} / P_m$, where P_m and I_{mp} denote maximum power and corresponding maximum power current respectively [30]. For illustration, we present simulation results (see Fig.3.10), which show that α stays relatively constant over a wide range of temperature/insolation. To implement this idea, a periodic interrupt routine is build into the proposed MPPT algorithm. In the periodic interrupt the expected maximum power P_m is computed using

$$P_m = \alpha * I_{pv}, \quad (3.8)$$

where I_{pv} stands for the present value of the operating current. The algorithm then checks if P_m is comparable to the actual output power P_o as in Eq. (3.9), which is one way to ensure the operation at the global power peak. If this condition is not met, a modified P&O will be used to track the global peak.

$$P_m - P_o < \xi, \quad (3.9)$$

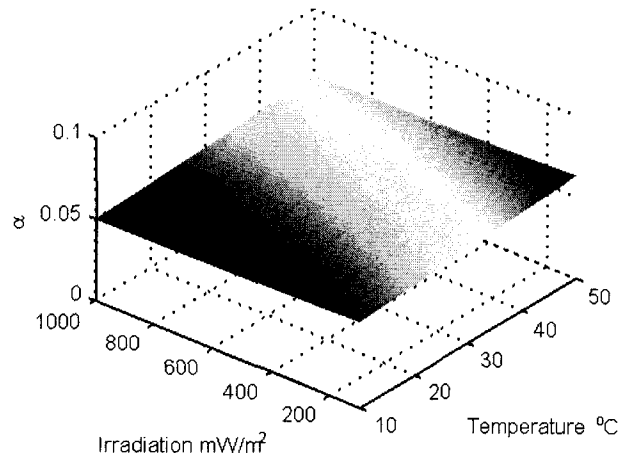


Figure 3.10 Relationship between maximum power P_m and corresponding maximum power current I_{mp}

3.3. Flow Chart

The complete flow chart of the proposed algorithm is shown in Fig.3.11. First, the algorithm commences by setting initial values to voltage, current, and duty-cycle and (*i.e.* $V_{pv}[k]$, $I_{pv}[k]$, and $D[k-1]$); in addition, it sets a starting value to the duty-cycle $D[k]$. Afterwards, the algorithm loop starts by sensing the output voltage $V_{pv}[k]$ and current $I_{pv}[k]$ of the PV module. This allows the algorithm to compute the output power of the PV module using $P_o[k] = V_{pv}[k] * I_{pv}[k]$. Next, the main parameters of the MPPT algorithm are calculated which are $dP[k]$ and $dD[k]$. Using those two parameters, the relative position of the operating point with respect to the MPP is determined by the sign of $dP[k]/dD[k]$ (refer to Fig.3.5). Consequently, this guides the direction of the next duty-cycle update.

After determining the next direction of the duty-cycle, the adaptive step-size value is to be computed using the proposed approach (*i.e.* using the first and second derivative of P - D function). For that purpose, the second derivative $\Delta(dP[k]/dD[k])$ sign is computed using Eq. (3.3). Using this sign and the value of the first derivative $dP[k]/dD[k]$, the operating region can be determined (*i.e.* I, II, III or IV), and the step-size $a(k)$ is updated using Eq. (3.5).

Followed by that, the second characteristic of the proposed algorithm comes into action, which is the separation of power change $dP[k]$ into components $dP_1[k]$ and $dP_2[k]$ using Eq. (3.6) and Eq. (3.7). Then $dP_1[k]$ and $dP_2[k]$ are compared to take into consideration the effect of rapidly changing atmospheric conditions. The duty-cycle direction is reversed if $dP_2[k] > dP_1[k]$. Finally the reference variable $D(k)$ is updated by $a(k)$ and the algorithm repeats periodically.

Meanwhile, the interrupts (*i.e.* multiple peaks detection) are executed periodically to ensure the operation at the global maximum. The expected maximum power P_M is calculated using Eq. (3.8), and then it is compared to the actual output power P_o using Eq. (3.8) to ensure the operation at the global maximum.

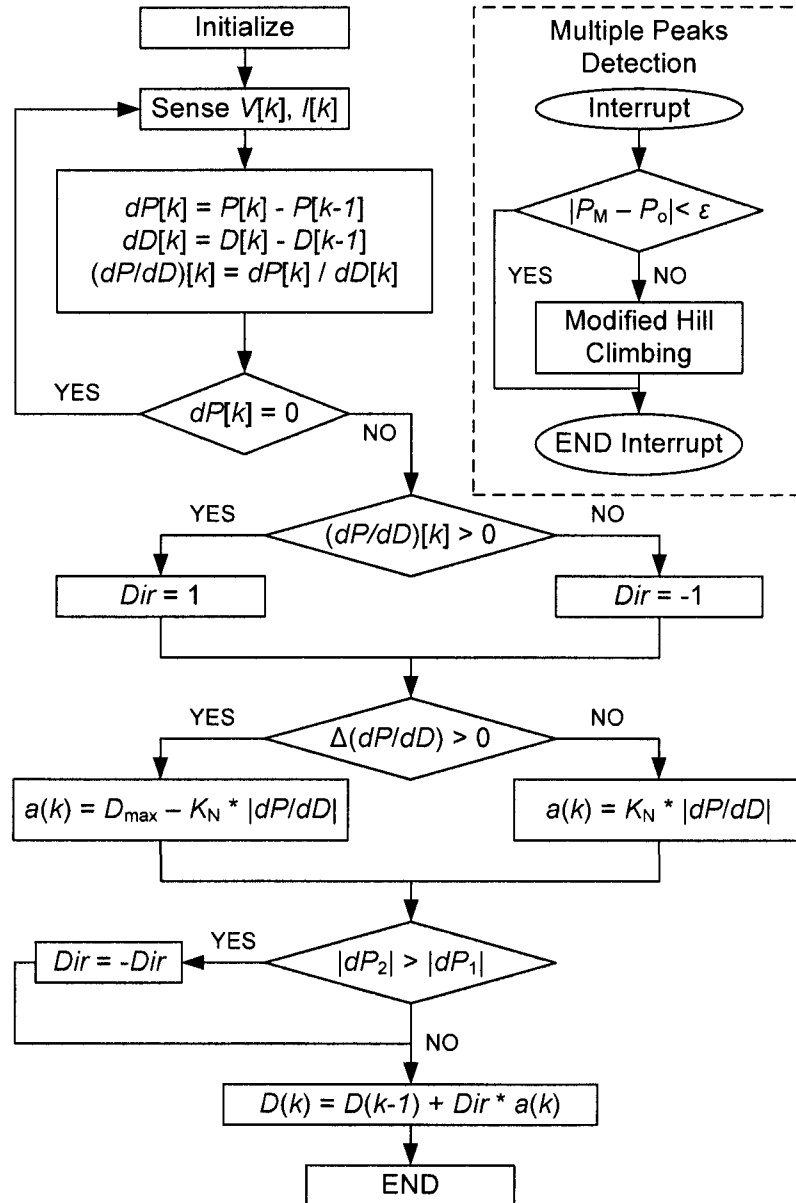


Figure 3.11 Flow chart of the proposed algorithm

3.4. Conclusion

In this chapter, the proposed maximum power point tracking algorithm has been presented and analyzed. A modified rule for updating the reference variable has been proposed. The issue of rapidly changing atmospheric condition has been addressed by the by introducing a null current measurement. Moreover, the effect of partial shading has been resolved using periodic interrupts to detect such regions. Finally the flow chart of the complete algorithm has been presented and discussed.

Chapter 4. Simulation and Experimental Results

4.1. Introduction

In this chapter, a SIMULINK model will be implemented to test and verify the functionality of the proposed algorithm. The results under the standard test conditions will be presented and compared to the response of P&O algorithm under different step-size values of the reference variable (*i.e.* duty-cycle). Moreover, different irradiation schemes will be tested with the proposed algorithm to test its dynamic response. The results will then be compared to an adaptive P&O algorithm and an adaptive ICM.

In addition, a hardware prototype will also be implemented using a micro-controller and a buck converter. The hardware schematic and parameters design will also be analyzed. Experimental results will be presented under a constant irradiation level; these results will then be compared to an adaptive P&O algorithm.

4.2. SIMULINK Setup

4.2.1 Developed Model of PV Panels

The PV panel is modeled in SIMULINK as a current controlled voltage source (CCVS), shown in Fig.4.1, where the panel's current I_{pv} is the input and its voltage V_{pv} is the output. Moreover, two additional inputs were added (*i.e.* insolation and temperature) to study the module's response under various weather conditions.

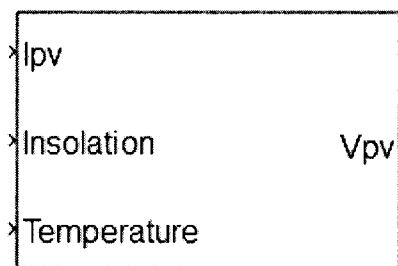


Figure 4.1 Modified SIMULINK model of PV modules

The detailed developed model of the PV panel is shown in Fig.4.2. As can be seen, the basic building block of this model is the node A traversed by the four currents (I_g , I_d , I_{sh} , and I_{pv}). These four current are those presented in the circuit model of PV cells (see Fig.4.3).

The current I_{pv} is calculated from the external circuit parameters and fed to the model, the current I_g is computed using a scaled value of the insolation input, and the currents I_d and I_{sh} are contingent on V_A . Consequently, the output of the node A is fed to an algebraic constraint equation solver, which solves for an adequate value of V_A that satisfies Kirchhoff's current law (KCL) at this node.

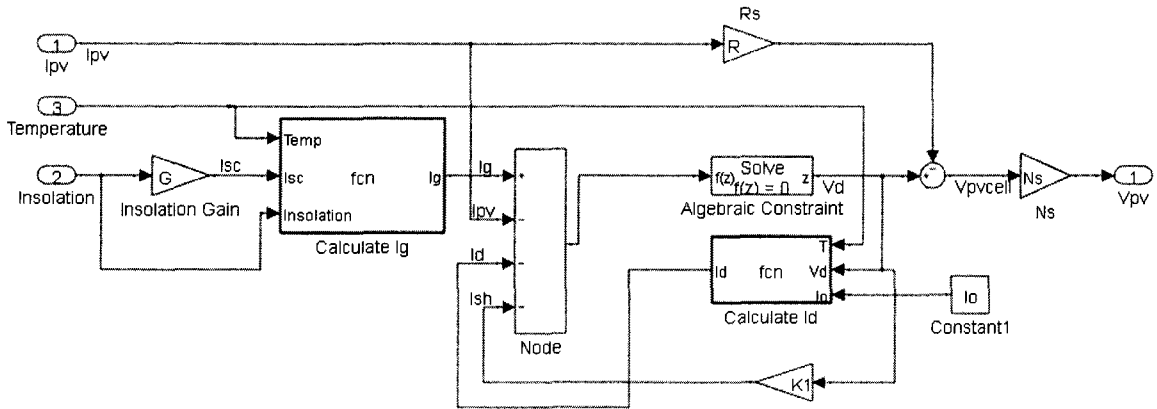


Figure 4.2 Modified SIMULINK model of PV modules (detailed view)

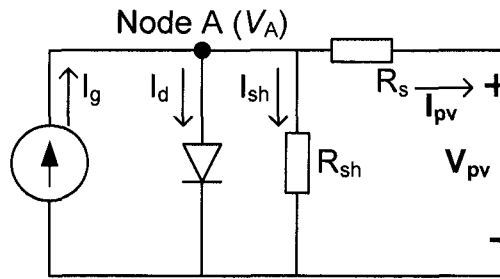


Figure 4.3 Circuit model of PV cells

Every PV panel can be characterized by four parameters to determine its I - V characteristics. These parameters, which are usually provided by the datasheet of the PV panel, are the open circuit-voltage V_{oc} , the short-circuit current I_{sc} , the maximum power voltage V_{mp} , and the maximum power current I_{mp} .

To verify the functionality of the model, the system in Fig.4.4 is implemented. The parameters of the PV panel are designed such that the following specifications of the panel are met: $V_{oc} = 22.2V$, $I_{sc} = 5.45A$, $V_{mp} = 17.2V$, and $I_{mp} = 4.95A$ (selected from a datasheet). A current sweep from zero to the short-circuit current I_{sc} is fed to the PV panel model at an insolation of $1000W/m^2$ and a temperature of $25^\circ C$. The output voltage and the output power with respect to the current input are displayed in Fig.4.5.

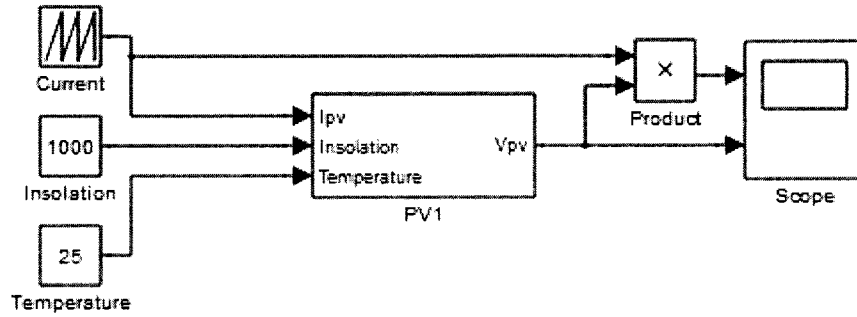


Figure 4.4 SIMULINK test system of PV modules

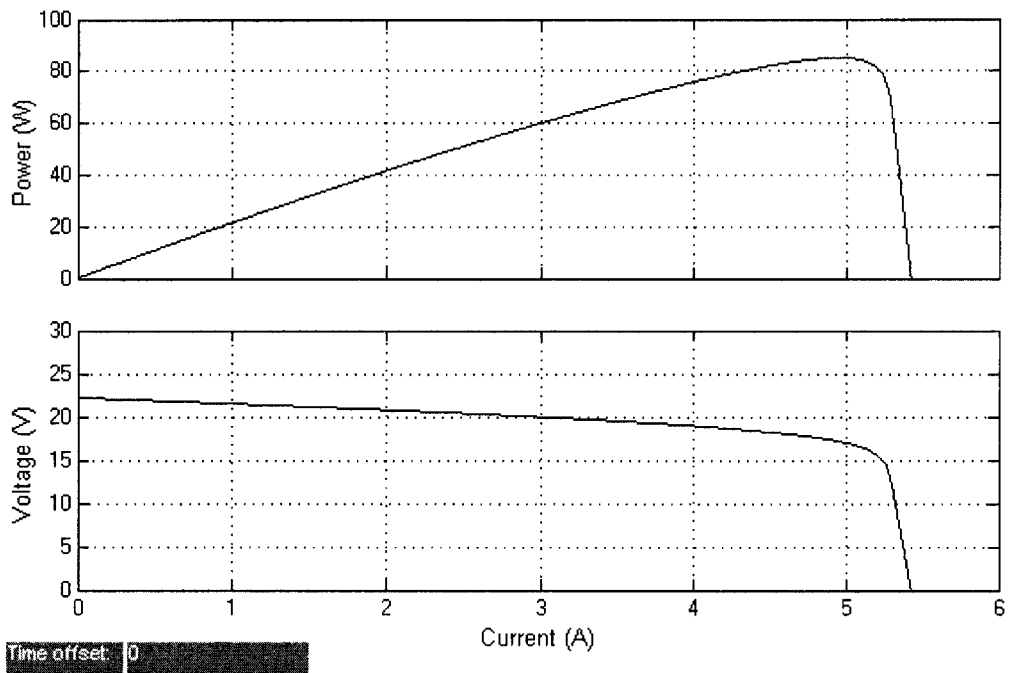


Figure 4.5 $I-V$ and $P-I$ characteristic of the PV model

A comparison between the desired specifications and the results obtained by the model show that the model provides a high degree of accuracy in mimicking the behaviour of a PV panel. To further test the presented model, the same system in Fig.4.4 is simulated under different insolation levels and the results of the $I-V$ characteristics are shown in Fig.4.6.

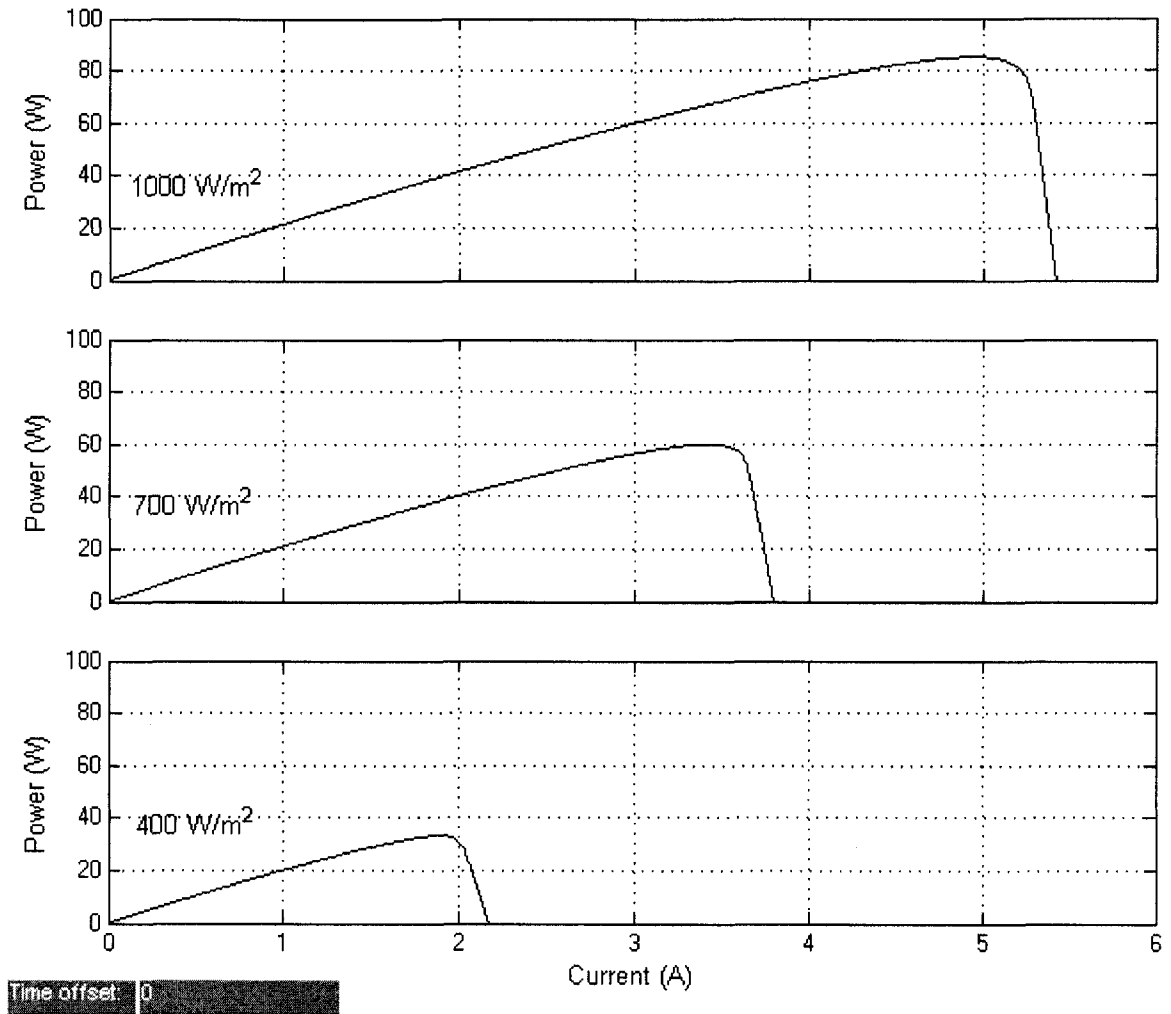


Figure 4.6 P-I characteristics under different insolation levels

The results in Fig.4.6 verify the functionality of the panel's model under different insolation levels. The short-circuit current of the PV module decreases as the insolation level drop from $1000W/m^2$ to $400W/m^2$. In conclusion, the $I-V$ and $P-I$ curves resulted from the presented model of PV panels provides an excellent approximation to the realistic model. This PV panel model will be used to test the proposed MPPT algorithm and some conventional algorithms for comparison purposes.

4.2.2 Buck Converter Modeling

The theoretical model of the buck dc-to-dc converter is used in the SIMULINK system. The converter schematic is shown in Fig.4.7, and the design formulas of the buck components are listed in Eq. (4.1)-(4.4) [31]. The value of the inductor L_1 should be large enough to operate the converter in the continuous mode and is calculated as,

$$L_1 \geq \frac{V_{om}(1 - D_{mp})}{f_s |\Delta I_L|}, \quad (4.1)$$

where V_{om} is the maximum output voltage, D_{mp} is the duty-cycle corresponding to the maximum power output, f_s is the switching frequency, and ΔI_L is the peak-to-peak ripple of the inductor current.

The output capacitor C_2 is designed to have a low voltage ripple at the output, and its value is computed using

$$C_2 \geq \frac{D_{mp} I_{om}}{r f_s V_{om}}, \quad (4.2)$$

where I_{om} is the dc component maximum output current, and r is the ripple factor which is defined as

$$r = \frac{\Delta V_o}{V_{om}}, \quad (4.3)$$

Finally the input capacitor is designed such that the current ripple at the converter's input is less than 2%. The capacitor C_1 is designed using

$$C_1 \geq \frac{(1 - D_{mp}) I_{om} D_{mp}}{0.02 V_{mp} f_s}. \quad (4.4)$$

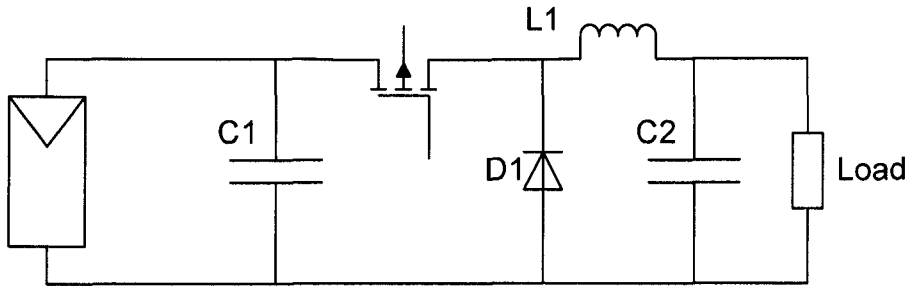


Figure 4.7 Schematic of the buck DC-to-DC converter

The buck converter is designed to operate in the continuous mode with the following specification: the output voltage ripple is less than 2%, the input current ripple less than 2%, and the peak-to-peak inductor current ripple is 0.05A. The computed values using Eq. (4.1)-(4.2) are: $L_1=1mH$, $C_1=220\mu F$, $C_2=220\mu F$, $R=1\Omega$, and the switching frequency f_s is 100KHz. The buck converter test system is shown in Fig.4.8 and the resulting voltages and currents are shown in Fig.4.9. As can be seen from this result, the ripples in the voltages and currents satisfy the design constraints.

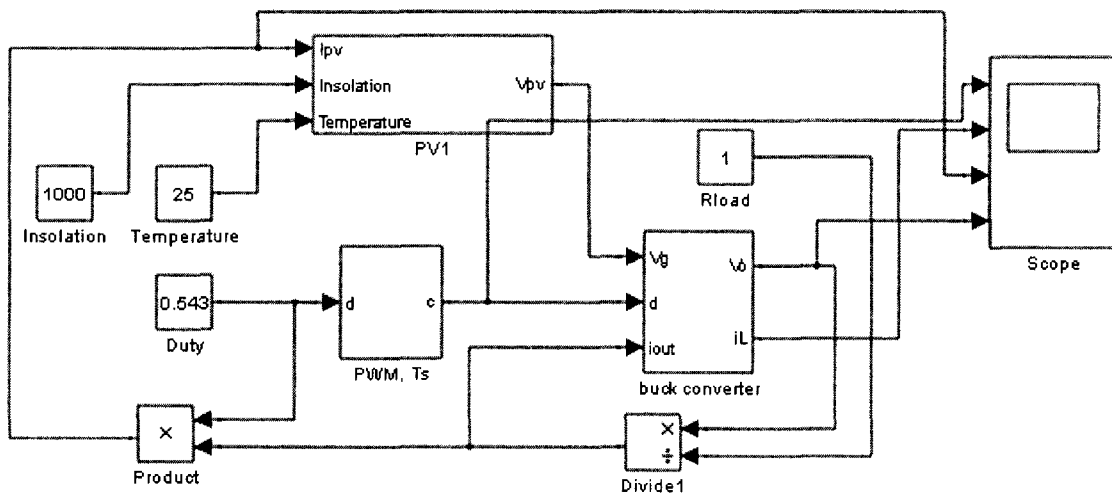


Figure 4.8 SIMULINK test system of the buck converter

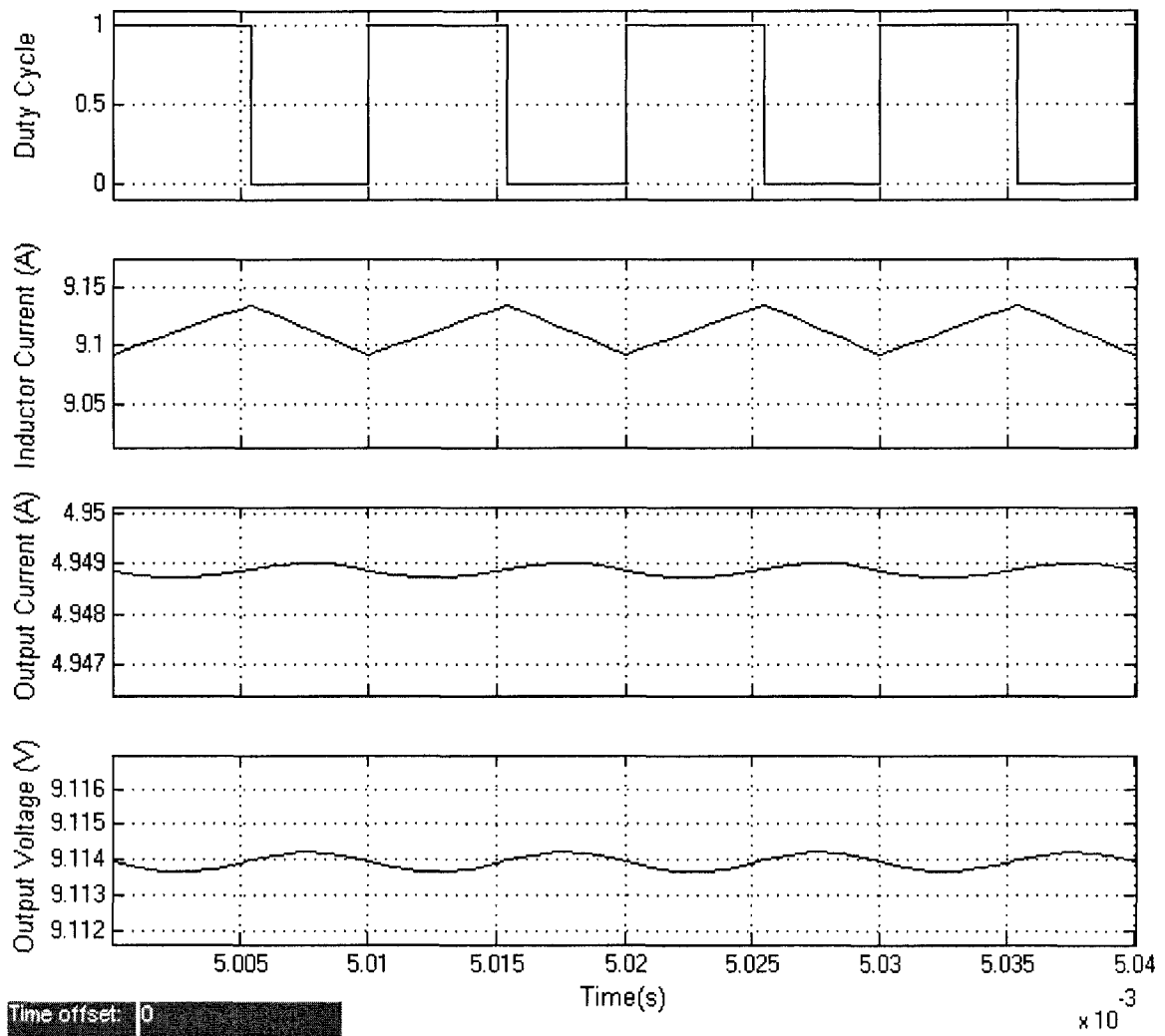


Figure 4.9 Simulation results of the buck converter model

4.2.3 Complete SIMULINK Model

The complete SIMULINK model of the PV system is shown in Fig.4.10. The modeled system consists mainly of the developed model of PV panels, the theoretical model of the buck converter, and a load. In addition, it contains a MATLAB function block to implement the proposed algorithm. Finally, a multi-input scope is included to display the resulted output.

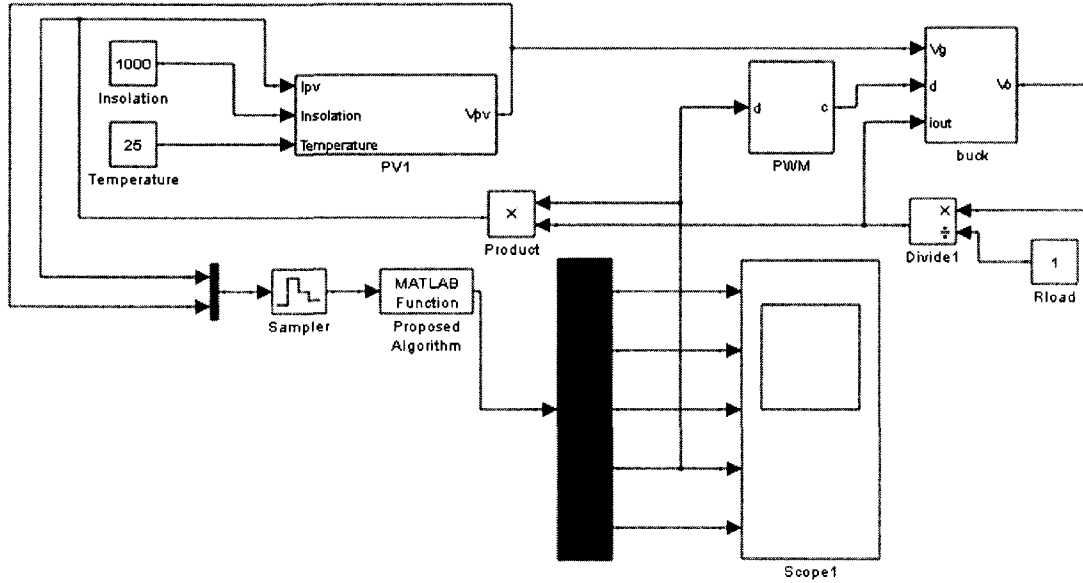


Figure 4.10 Complete SIMULINK model of the PV system

The MATLAB function block accepts the panel's voltage V_{pv} and current I_{pv} as inputs through a multiplexer. These inputs are then fed to sample-and-hold block which samples the voltage and current periodically on a pre-set sampling frequency of 10KHz. The MATLAB function block processes the voltage and current data using the built-in function of the proposed algorithm. Since the reference variable chosen is the duty-cycle, the output of this function block is the duty-cycle D_k which is fed directly into the buck converter.

The output voltage V_{pv} of the module is fed into the buck converter and processed according to the duty-cycle D_k . The output voltage V_o of the converter is used to calculate the output current I_o of the converter (*i.e.* $I_o = V_o/R$). Consequently, the module's current can be calculated using,

$$I_{pv} = I_o * D_k \quad (4.5)$$

4.3. Transient /Steady-state Response Results and Discussions

The SIMULINK system with the proposed algorithm was simulated under the standard test conditions (*i.e.* insolation= $1000W/m^2$, and temperature= $25^{\circ}C$). The specifications of the PV panel were set as follows, $V_{oc}=22.2V$, $I_{sc}=5.45A$, $V_{mp}=17.2V$, and $I_{mp}=4.95A$. This corresponds to maximum power output P_M of $85.14W$ ($P_M=I_{mp}*V_{mp}=85.14W$). The simulation results of the significant outputs of the modeled system are shown in Fig.4.11. The presented results prove the functionality of the proposed adaptive step-size update presented in chapter 3, specifically in Eq. (3.4).

The initial value of the duty-cycle chosen was far enough from the optimum duty-cycle in order to observe the tracking process. By analyzing the results, one can see that in the time interval where the function dP/dD function is increasing (*i.e.* $t < 3ms$), the algorithm could identify the operating region (*i.e.* region I), and update the step-size according to Eq. (3.4). In this region, the step-size update is inversely proportional to the magnitude of dP/dD , hence the step-size decreases in this region as we approach region II. In this second region (*i.e.* when dP/dD is decreasing), the step-size update is directly proportional to the magnitude of dP/dD ; consequently, the step-size starts decreasing and attains its minimum when the maximum power point MPP is reached.

The maximum power point is reached at $4ms$, in this time interval (*i.e.* $4ms < t < 10ms$) the operating point is fluctuating between regions II and III (refer to Fig.3.5). Since the value of dP/dD is very small, the step-size value is set to minimum in this time interval. The output voltage and current of the PV module are shown in Fig.4.12, the maximum power voltage V_{mp} and maximum power current I_{mp} are also attained in this steady-state time interval (*i.e.* $4ms < t < 10ms$).

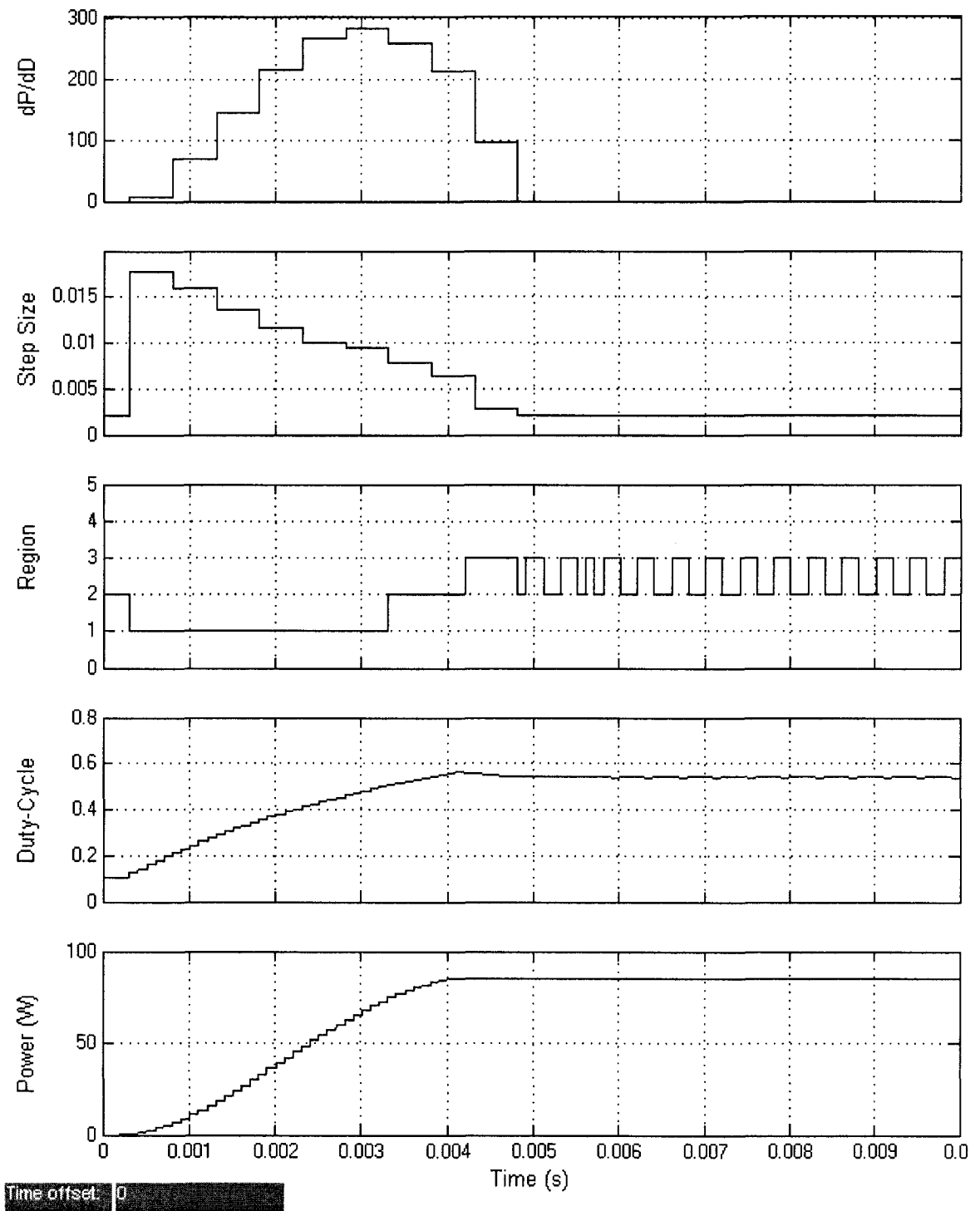


Figure 4.11 Significant outputs of the modeled PV system

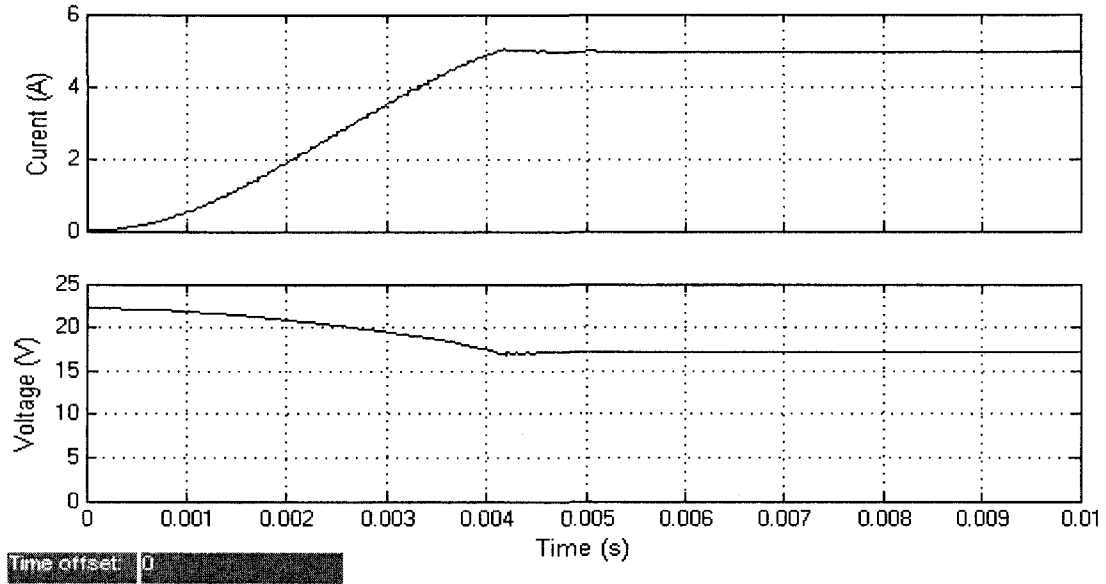


Figure 4.12 Simulation results of the output voltage and output current of the PV module

4.3.1 Comparison with P&O Algorithm

To evaluate the performance of the proposed algorithm, its response was first compared to the Perturb and Observation (P&O) algorithm. The comparison was done with three different step-size values (a_k) of the P&O algorithm 0.005, 0.008 and 0.015. Note that the step-size values corresponds to the duty-cycle since it is the reference variable. In each case, the response of the P&O algorithm is presented and compared to the response of the proposed algorithm. Followed by that, the error from the ideal case is presented for both algorithms, and the average error is calculated for comparison purposes. The results are presented in Fig.4.13-4.20, and the overall comparison is presented in Fig.4.21-4.22 and summarized in Table 4.1. The simulation was done under a constant insolation and temperature levels. The simulation runtime was 10ms, where the purpose is to verify the improvements in the transient and steady-state response of the proposed algorithm.

a) Step-size = 0.005

The first comparison case is with the P&O algorithm where the step-size is set to 0.005, which is a relatively small value. The responses of the two algorithms are shown in Fig.4.13; the P&O algorithm attains the maximum power at 9ms, as the proposed algorithm attains it at 4ms. The maximum targeted power at the selected simulation conditions is 85.14W, and this is set as an ideal case to calculate and compare the error in the tested algorithms. The error between the ideal response and that of the P&O response is shown in Fig.4.14 (a), where the average error was calculated to be 0.3944. The error between the ideal output and that of the proposed algorithm response is shown in Fig.4.14 (b), where the average error is calculated to be 0.1857. This corresponds to an efficiency improvement of 31.35% which is mainly in the transient response. The small step-size in the P&O leads to a slow transient response but to a stable steady-state response. However, the adaptive step-size in the proposed algorithm can match the performance of the small step-size P&O, and leads it by its fast transient response.

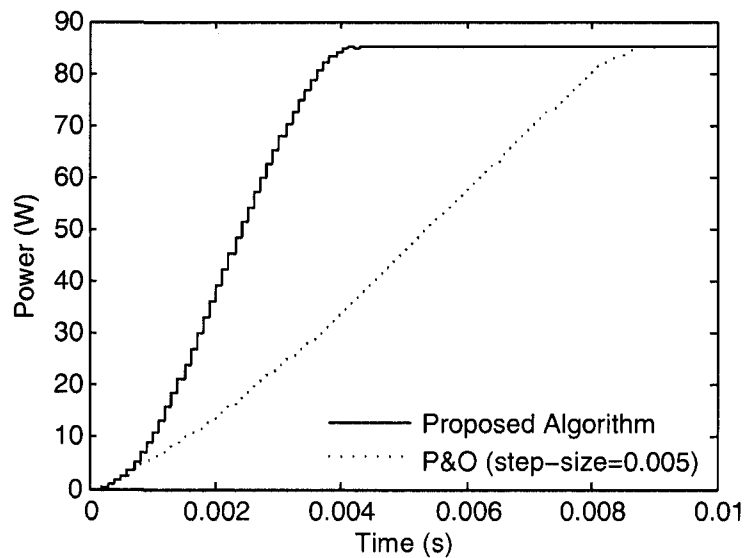


Figure 4.13 Comparison between the proposed algorithm and P&O with step-size = 0.005

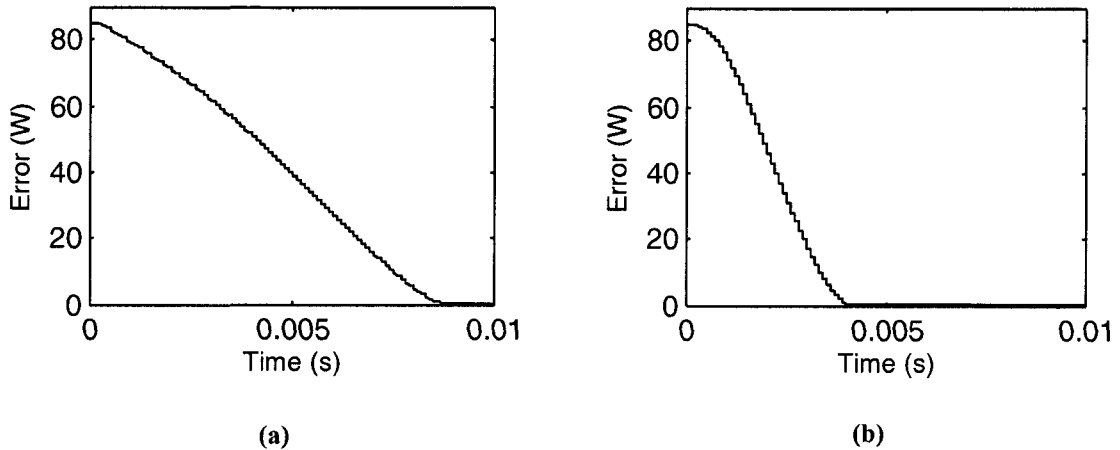


Figure 4.14 Error from the ideal case in (a) P&O (step-size=0.0005), (b) proposed algorithm

b) Step-size = 0.008

For the second comparison case, a medium step-size value (0.008) is selected for the P&O algorithm. The same comparison procedure as the first case is followed, and the simulation results are shown in Fig.4.15. The proposed algorithm attains the maximum power at 4ms, while the current P&O attains it at 5.6ms. This larger step-size in the P&O leads to a better transient response than the first case, but small power oscillations appear in the steady-state which can cause significant power loss in the long run. The error between the ideal response and that of the P&O response (step-size=0.008) is shown in Fig.4.16 (a), where the average error was calculated to be 0.2609. The error between the ideal response and that of the proposed algorithm response is shown in Fig.4.16 (b), where the average error is calculated to be 0.1857. This corresponds to an efficiency improvement of 11.3%, where the considerable part of this improvement is the transient response with a minor improvement in the steady-state response.

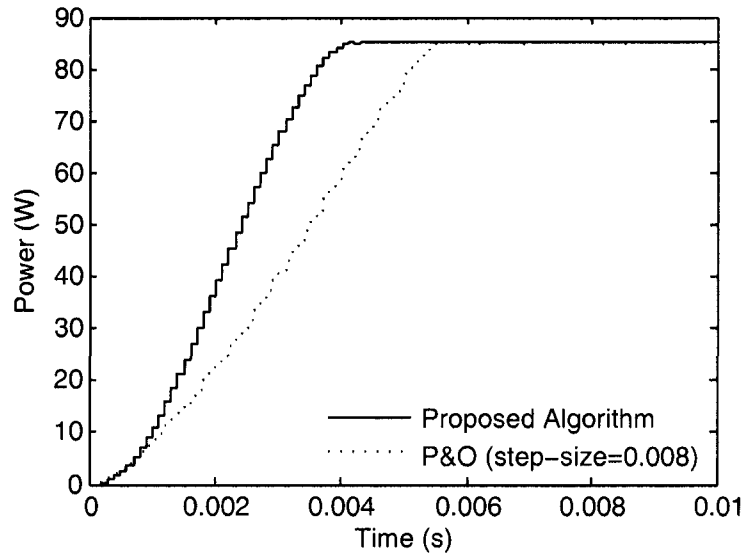


Figure 4.15 Comparison between the proposed algorithm and P&O with step-size = 0.008

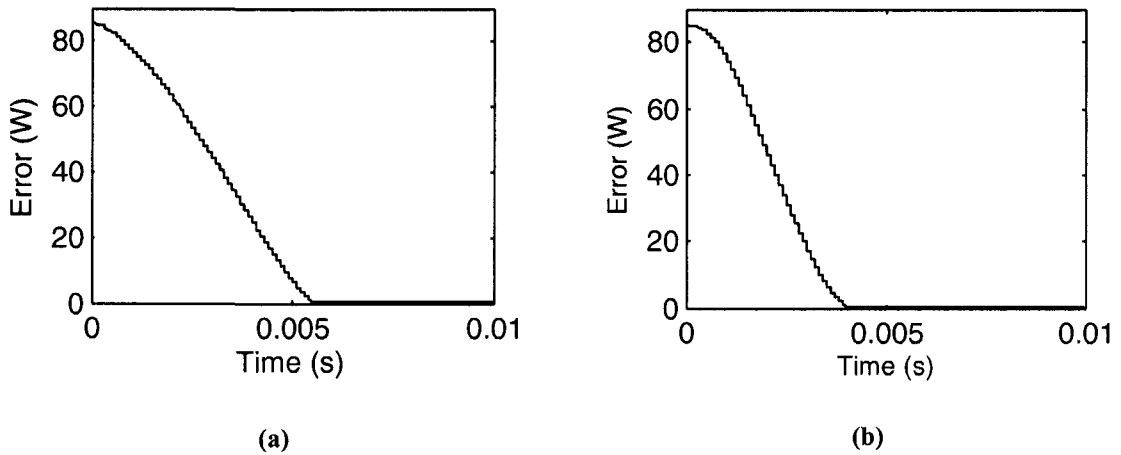


Figure 4.16 Error from the ideal case in (a) P&O (step-size=0.008), (b) proposed algorithm

c) Step-size = 0.015

The final comparison case with the P&O algorithm is done for a large fixed step-size (0.015). The simulation results are shown in Fig.4.17, where the proposed algorithm attains the maximum power at 4ms, while the current P&O attains it at 4.4ms. The error between the ideal response and that of the P&O response is shown in Fig.4.18 (a), where the average error was calculated to be 0.2129. The error between the ideal response and

that of the proposed algorithm response is shown in Fig.4.18 (b), where the average error is calculated to be 0.1857. This corresponds to an efficiency improvement of 4.09%, with a significant improvement in the steady-state response.

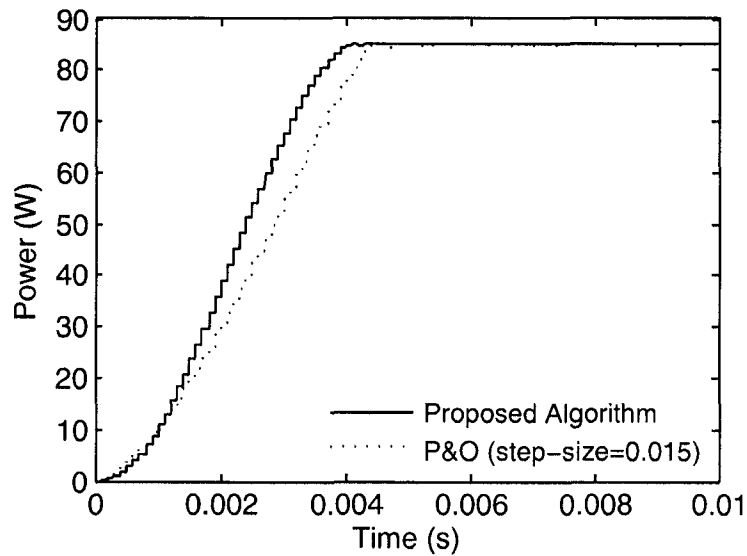


Figure 4.17 Comparison between the proposed algorithm and P&O with step-size = 0.015

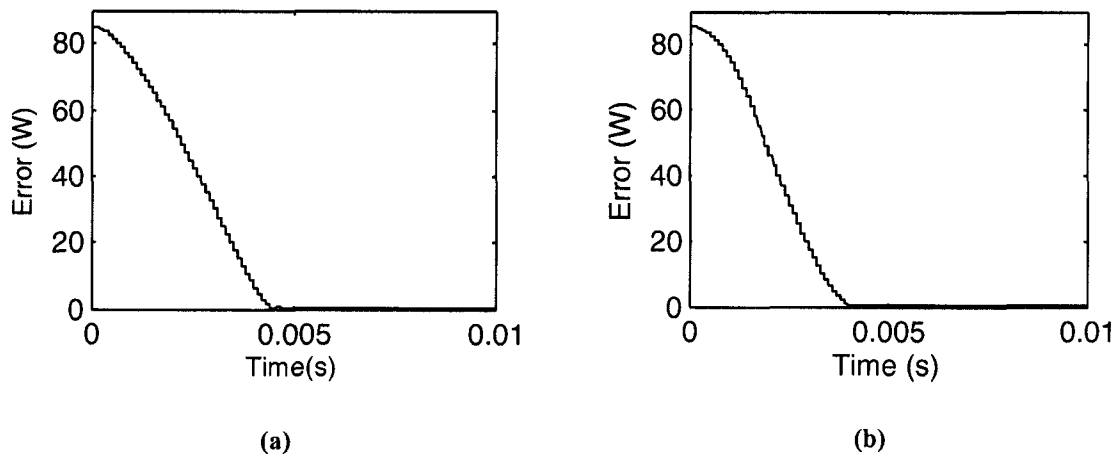


Figure 4.18 Error from the ideal case in (a) P&O (step-size=0.015) (b) proposed algorithm

To further analyze the steady-state response of this specific case (step-size=0.015), a magnified view of the steady-state response is presented in Fig.4.19. The results clearly show the large power oscillations when a large step-size is used in the

P&O algorithm. The steady-state error between the ideal response and that of the P&O response (step-size=0.015) is shown in Fig.4.20 (a), where the average error was calculated to be $6.4e-4$. The error between the ideal response and that of the proposed algorithm response is shown in Fig.4.20 (b), where the average error is calculated to be $4.2e-5$. This corresponds to an efficiency improvement of 0.18% in the steady-state response, which can lead to significant gain on the long run.

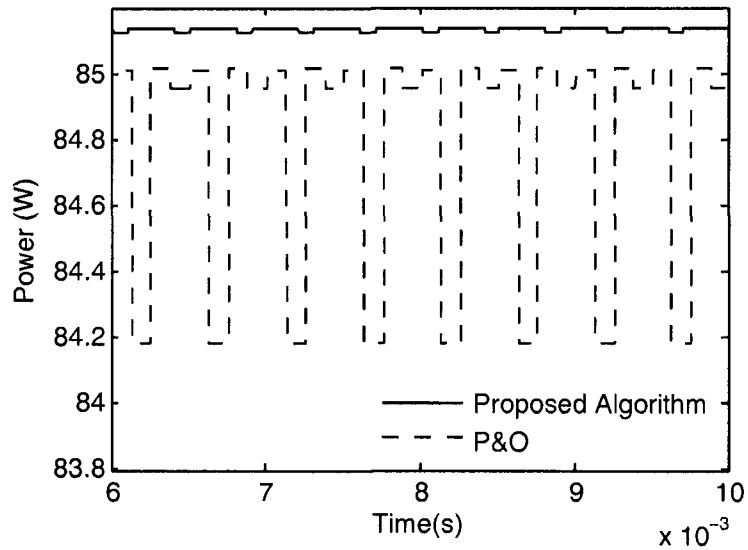


Figure 4.19 Steady-state comparison between the proposed algorithm and P&O with step-size = 0.015

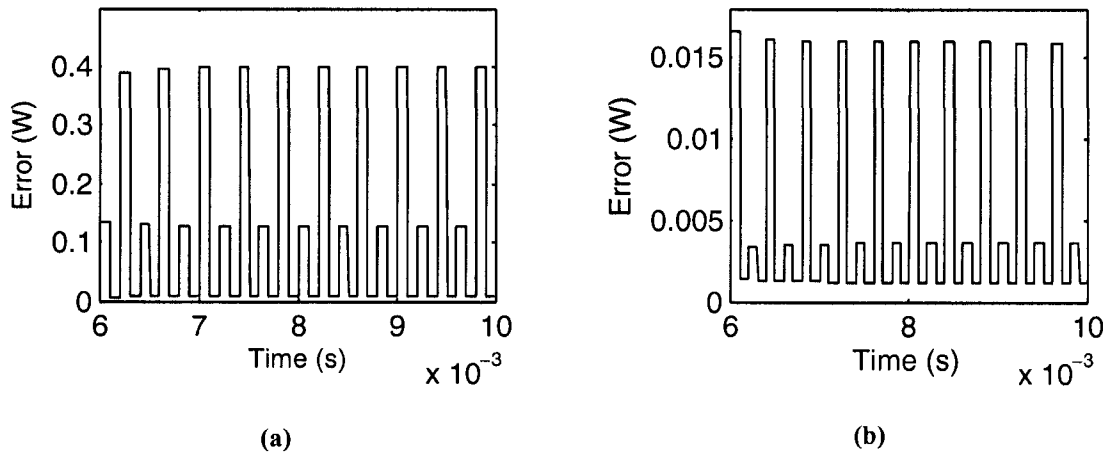


Figure 4.20 Steady-state error from the ideal case in (a) P&O (step-size=0.015) (b) proposed algorithm

d) Overall Comparison

To conclude this section, we present in Fig.4.21-4.22 a comparison among the error functions of all the tested algorithms, and a summary in Table 4.1. The improvement in the transient response is clearly shown in Fig.4.21, where the proposed algorithm has the least error compared to the P&O algorithm (with different step-size values). The best transient response of the P&O algorithm is with the largest step-size (0.015); however, the larger the step-size the bigger the steady state oscillations. The steady-state response of this particular algorithm (*i.e.* P&O with step-size of 0.015) and that of the proposed algorithm are presented in Fig.4.22. As can be seen from this comparison, the large step-size which led to the best transient response resulted in significant power oscillation at the steady-state.

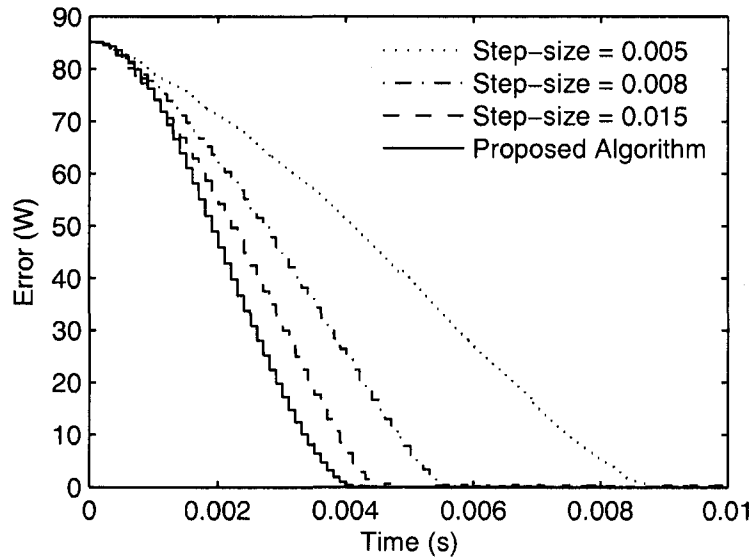


Figure 4.21 Error comparison among the proposed algorithm and different P&O algorithms

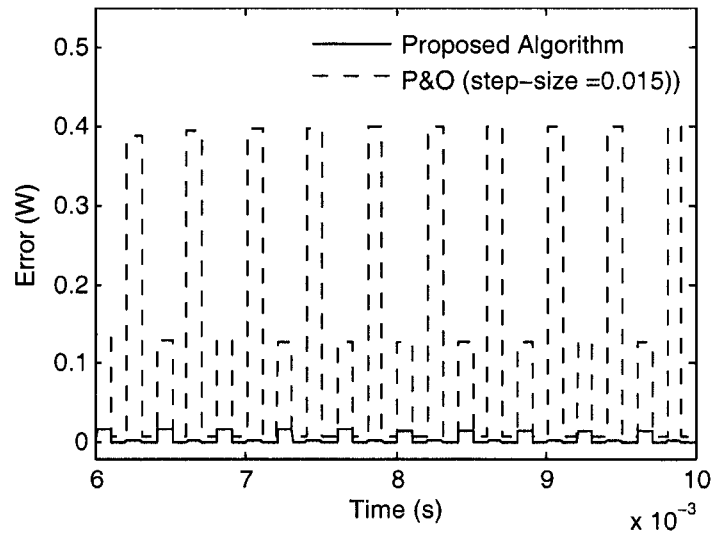


Figure 4.22 Steady error comparison between the proposed algorithm and P&O (step-size=0.015)

Table 4.1 summarizes the efficiency improvement in the proposed algorithm with respect to the three tested algorithms. The efficiency improvement is divided between that of the transient response and the steady-state response. The maximum efficiency improvement achieved in the steady-state response is 0.18%, which is over the P&O (with step-size = 0.015). The maximum efficiency improvement achieved in the transient response is 31.33%, which is over the P&O (with step-size = 0.005).

Table 4.1 Summary of the comparison cases with P&O algorithm

Step-size of the P&O Algorithm	Efficiency improvement by the proposed algorithm	
	Transient response	Steady-state response
Step-size = 0.005	31.33%	0.02%
Step-size = 0.008	11.21%	0.09%
Step-size = 0.015	3.91%	0.18%

4.4. Dynamic Response Results and Discussions

4.4.1 First Irradiation Scheme (Comparison with Adaptive P&O)

In this section, the algorithm is tested under varying insolation levels to verify its dynamic response and compare it to another algorithm. The first irradiation scheme chosen for testing is outlined in Fig.4.23. This scheme consists of: (1) an insolation level of $1000W/m^2$ in the time interval $0ms < t < 10ms$, (2) a uniformly descending insolation levels from $1000W/m^2$ at $t=10ms$ to $600W/m^2$ at $t=15ms$, (3) and an insolation level of $600W/m^2$ in the time interval $15ms < t < 25ms$.

This irradiation scheme was tested with the proposed algorithm, and an adaptive P&O (*i.e.* using the traditional adaptive step-size). The response of both algorithms is shown in Fig.4.23. The error between the ideal response and that of the adaptive P&O response is shown in Fig.4.24 (a), where the average error was calculated to be 0.2588. The error between the ideal response and that of the proposed algorithm response is shown in Fig.4.24 (b), where the average error is calculated to be 0.1860. This corresponds to an efficiency improvement of 3.19%.

The error comparison is shown in Fig.4.25, the proposed algorithm shows a significant improvement in the time interval $10ms < t < 15ms$. This time interval corresponds to the period of rapidly changing atmospheric conditions. In addition, the proposed algorithm shows a better transient response which can be seen in the time interval $4ms < t < 5ms$.

In summary, this comparison case showed the ability of the proposed algorithm to track the maximum power point under rapidly changing atmospheric condition (over a

descending insolation pattern). This is due to the introduction of the I_{null} current which studies the irradiation changes within the sampling period. Moreover, it showed the improvement of the proposed adaptive step-size (presented in chapter 3) over the traditional adaptive-size. In the next comparison case presented below, we test the algorithm on an ascending insolation pattern and a sudden insolation drop.

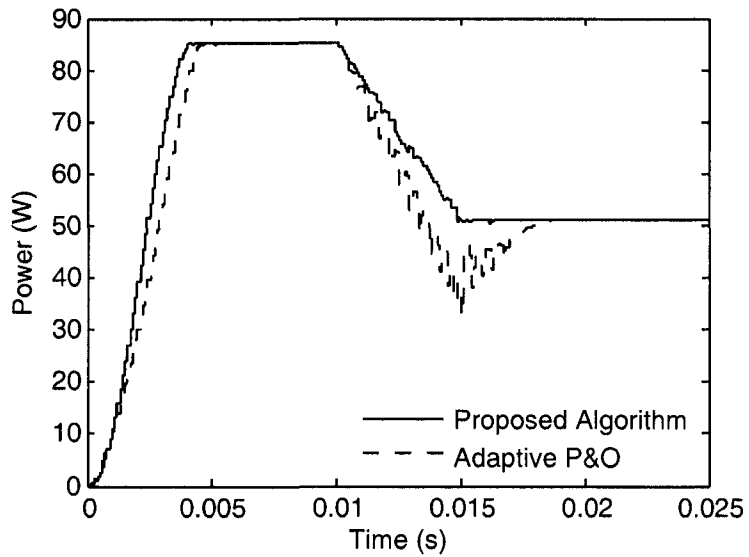


Figure 4.23 Comparison between the proposed algorithm and an adaptive P&O

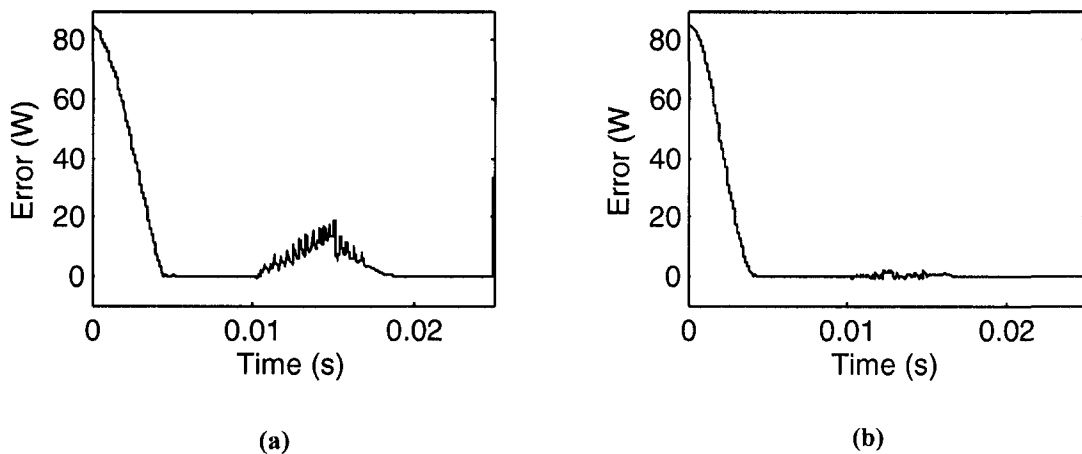


Figure 4.24 Error from the ideal case in (a) adaptive P&O (b) proposed algorithm

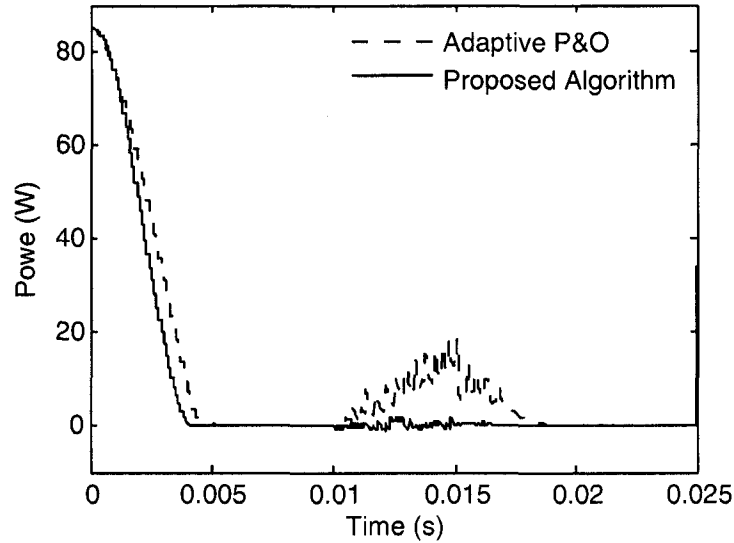


Figure 4.25 Error comparison between the proposed algorithm and an adaptive P&O

4.4.2 Second Irradiation Scheme (Comparison with Adaptive ICM)

The second irradiation scheme chosen for testing is outlined in Fig.4.26. This scheme consists of: (1) an insolation level of $1000W/m^2$ in the time interval $t=0ms$ till $t=10ms$, (2) a sudden insolation drop to $500W/m^2$ in the time interval $t=10ms$ till $t=20ms$, (3) a uniformly ascending insolation levels from $500W/m^2$ at $t=20ms$ to $1000W/m^2$ at $t=25ms$, (4) and an insolation level of $1000W/m^2$ in the time interval $25ms < t < 30ms$.

This irradiation scheme was also tested on the proposed algorithm, and an adaptive ICM (*i.e.* using the traditional adaptive step-size). The error between the ideal response and that of the adaptive ICM response is shown in Fig.4.27 (a), where the average error was calculated to be 0.2948. The error between the ideal response and that of the proposed algorithm response is shown in Fig.4.27 (b), where the average error is calculated to be 0.2439. This corresponds to an efficiency improvement of 2.87%.

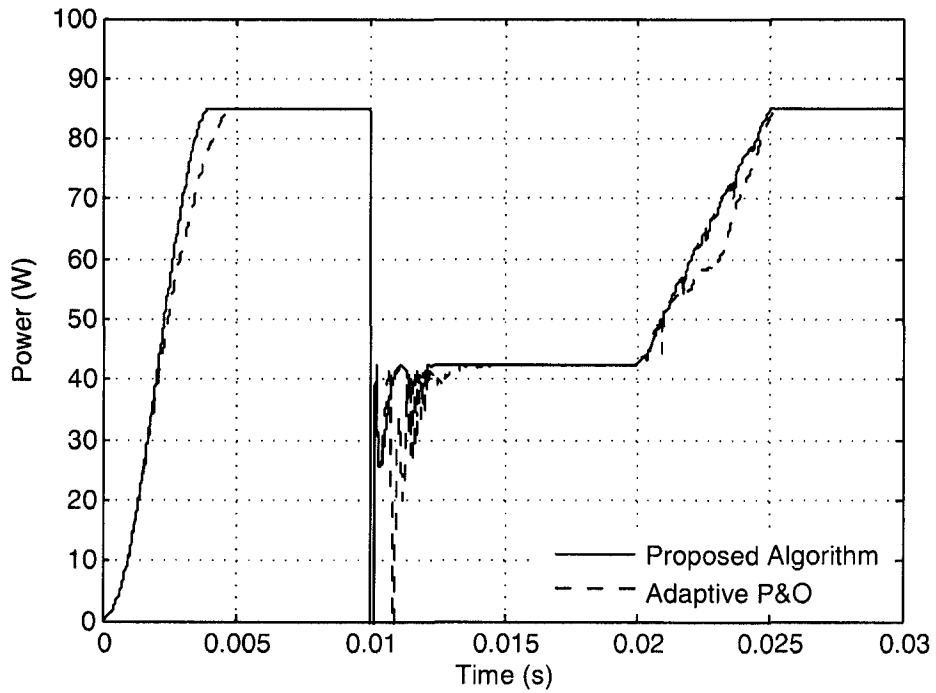


Figure 4.26 Comparison between the proposed algorithm and an adaptive ICM

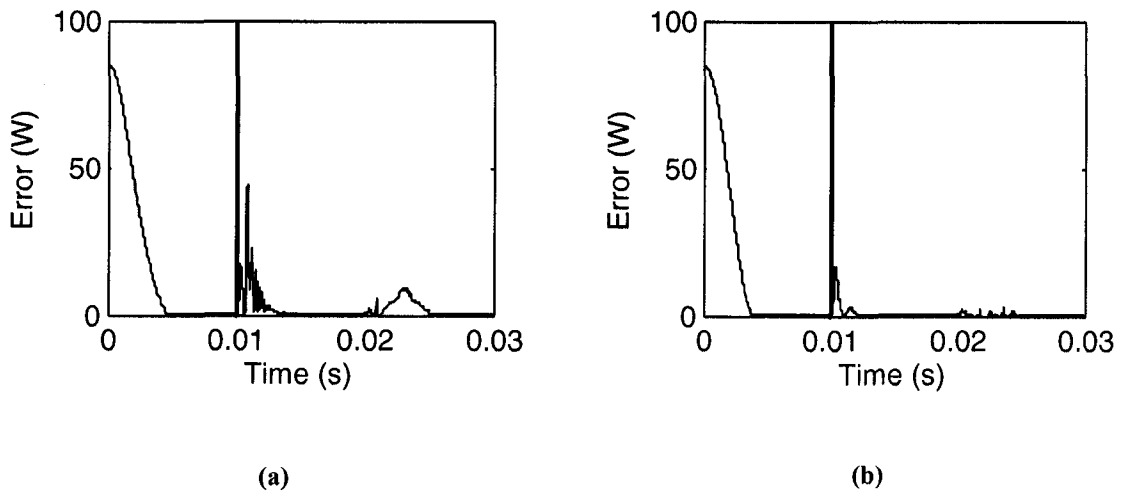


Figure 4.27 Error from the ideal case in (a) adaptive ICM (b) proposed algorithm

The error comparison is shown in Fig.4.28, the proposed algorithm shows a better transient response as illustrated in the time interval $0ms < t < 5ms$. In the time interval $10ms < t < 15ms$, the proposed algorithm shows a better recovery time after a sudden

insolation drop of $500W/m^2$. These enhancements are due to the advantages of the proposed adaptive step-size over the traditional adaptive step. Finally, in the time interval $20ms < t < 25ms$, the proposed algorithm shows a better tracking when we have fast ascending insolation levels, which also due to the introduction of I_{null} .

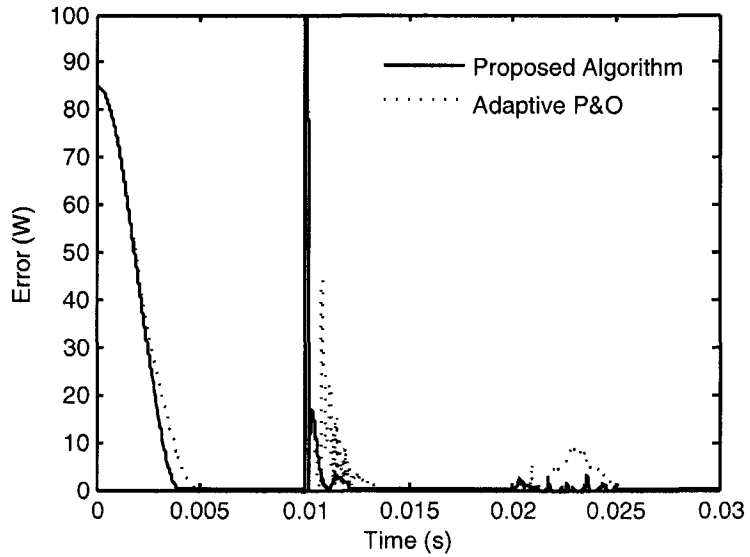


Figure 4.28 Error comparison between the proposed algorithm and an adaptive ICM

The improvements of the dynamic responses of the two cases presented in this section are shown in Table 4.2.

Table 4.2 Summary of the comparison cases with adaptive step-size algorithms

Irradiation scheme	Algorithm	Efficiency Improvement by the proposed algorithm (Dynamic Response)
Fast descending insolations	Adaptive P&O	3.19%
Sudden insolation drop + Fast ascending insolations	Adaptive ICM	2.87%

4.5. Experimental Setup

4.5.1 Overall Hardware Schematic

A schematic of the hardware design is shown in Fig. 4.29. The circuit consists of a PV module, a DC-DC converter, a micro-controller, voltage/current sensors, and other peripherals for ensuring the robustness of the system. The voltage/current sensors are used to periodically sample the panel's voltage and current. These sensors are passed to low pass filters (LPF) and voltage followers to improve the quality of the signal. Followed by that, these signals are fed into the micro-controller through the analog to digital (A/D) channels. The microcontroller process the voltage and current readings to calculate the direction and the value of the next step-size. The output of the micro-controller is the pulse-width-modulation (PWM) signal to control the buck DC-to-DC converter.

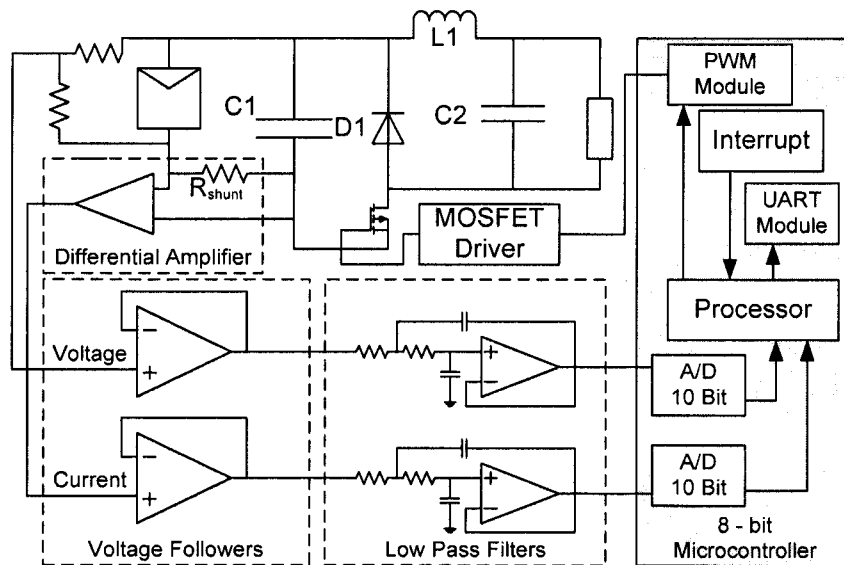


Figure 4.29 Hardware prototype schematic

The PV panel used in this research is an 85-Watt Kyocera (KC85T) panel, which consists of 36 PV cells. The electrical specifications of this module, at standard test conditions, are shown in Table 4.3, and its physical picture is shown in Fig.4.30. The current-voltage ($I-V$) characteristics and power-voltage ($P-V$) characteristics of the selected panel are given in the datasheet. The panel was tested using artificial lights in order to create a fixed test conditions for comparison purposes. Finally an LCD and a keypad were incorporated for user interface; the complete hardware setup is shown in Fig.4.31.

Table 4.3 PV panel specifications of the Kyocera KC85T

Parameter	Value
I_{mp}	5.02A
V_{mp}	17.4V
I_{sc}	5.34A
V_{oc}	21.7V
P_{max}	87W

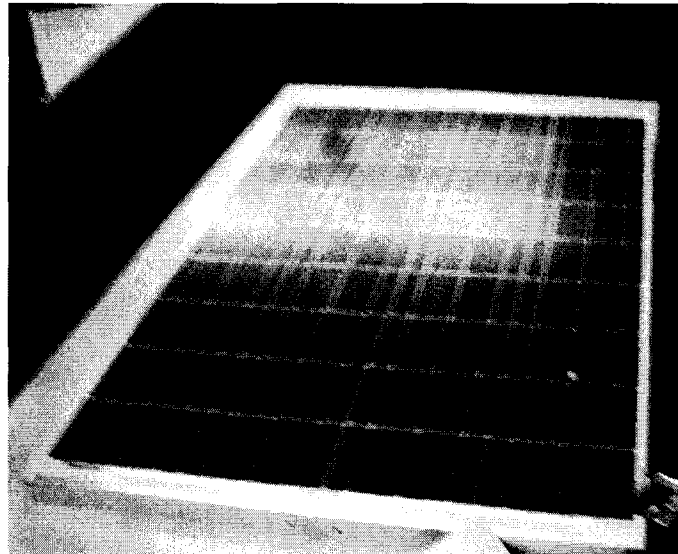


Figure 4.30 Kyocera 85Watt PV panel

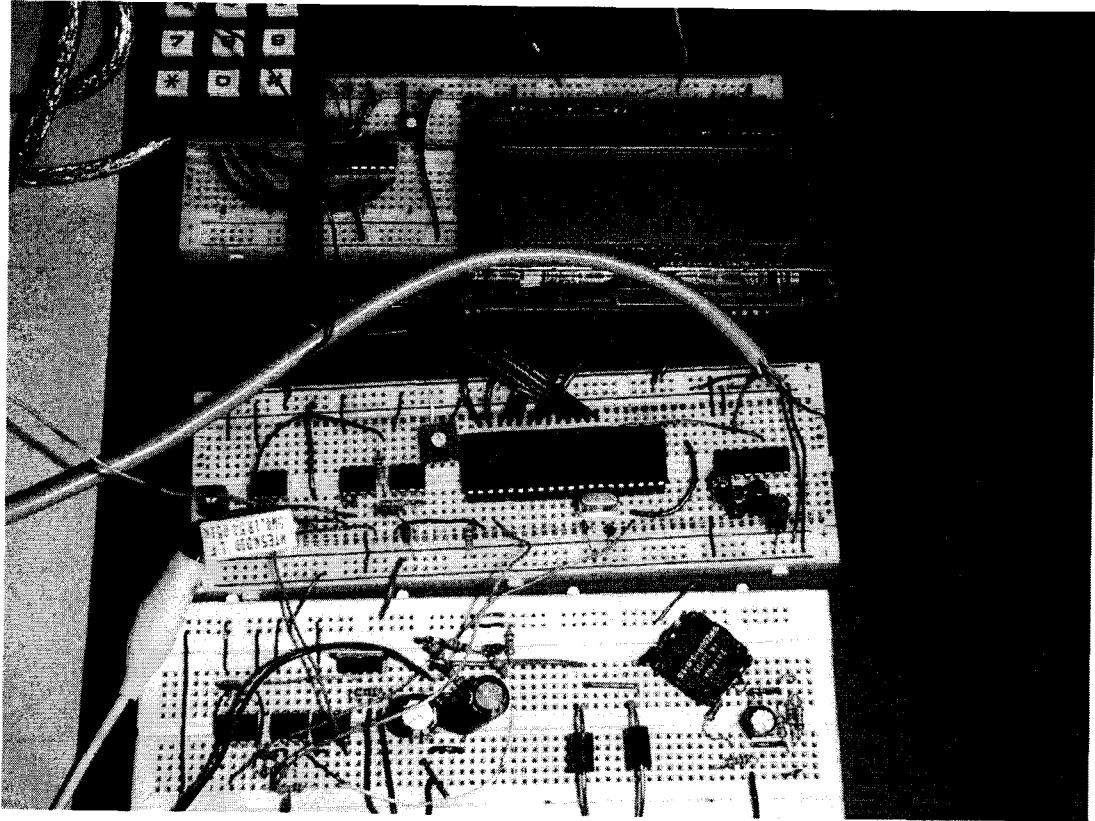


Figure 4.31 Actual hardware prototype

4.5.2 Voltage and Current Sensors

A voltage divider circuit is used to sense the module's voltage. The values of the resistors were chosen as high as possible (*i.e.* multiples of $100K\Omega$) in order to limit the current flow in the divider, thus minimizing power losses. The voltage divider must be designed such that its maximum output voltage does not to exceed $5V$ when the panel is operating at its maximum voltage (*i.e.* open-circuit voltage V_{oc}). The purpose of this is to protect the micro-controller which has a maximum limiting input voltage of $5.5V$.

As for the current sensor, a shunt resistor with a differential amplifier is used. This differential amplifier produces a voltage which is directly proportional to the current going into the PV module. Since the resistor is placed in series with the module, its value

was chosen as low as possible (0.1Ω) to minimize the power losses in this current sensing resistor. The gain of the differential amplifier was set such that its output voltage not to exceed $5V$ when the panel is operating at its maximum current (*i.e.* short-circuit current I_{sc}).

The sensors' outputs are passed to a voltage-follower in order to preserve the quality of the sampled signals. The signals are de-noised using second order low-pass filters (LPFs). The filters are derived from the Sallen & Key model with a unity gain. The selection of the cut-off frequency (f_c) satisfies $f_c \leq f_s/2$, in order to avoid the aliasing effect, where f_s is the sampling frequency. The schematic of the Sallen & Key is shown in Fig.4.32 [32],

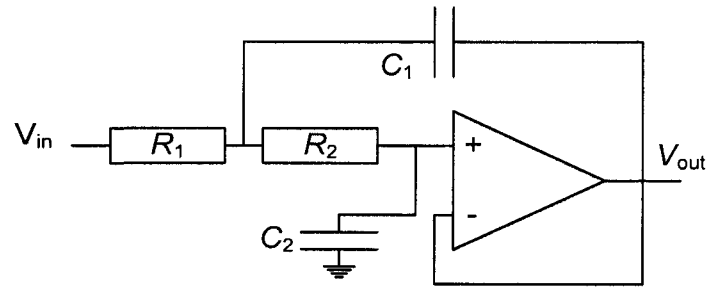


Figure 4.32 Sallen & Key low pass filter

and the cut-off frequency is set using [32]

$$f_c = \frac{1}{2\pi\sqrt{R_1 C_1 R_2 C_2}}, \quad (4.6)$$

and the quality factor Q is given by [32]

$$Q = \frac{\sqrt{R_1 C_1 R_2 C_2}}{(R_1 + R_2)C_2}. \quad (4.7)$$

4.5.3 Buck Converter

The DC-DC converter, which is the core of the MPPT unit, is a step-down buck converter. The converter's output LC filter is designed such that the converter operates in the continuous mode with low output voltage ripple (less than 2%). The same design formulas which were used for the buck converter in the SIMULINK model are used for the design of the experimental converter. However, the layout of the buck converter used in this experiment is shown in Fig.4.33. The current that corresponds to the on period (T_{on}) and off period (T_{off}) are shown in Fig.4.33 (a) and Fig.4.33 (b) respectively. The components used in this converter are listed in Table 4.4.

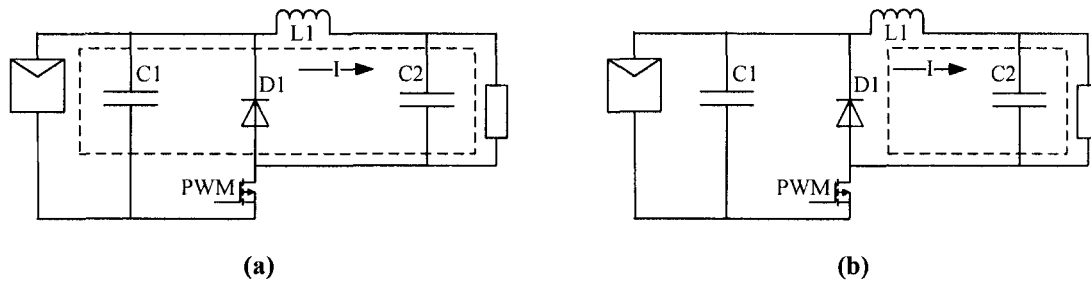


Figure 4.33 Buck converter current (a) T_{on} (b) T_{off}

Table 4.4 Components description of the buck converter

Component	Description
MOSFET	IRF740
MOSFET Driver	MAX4420
C_1	220 μF
C_2	220 μF
D_1	IN5408 (3A, $V_{RRM}=1000V$)
L_1	0.1mH

4.5.4 Microcontroller and Interface

The proposed MPPT algorithm was implemented on a PIC16F877A micro-controller. This micro-controller is an 8-bit architecture processor which contains all the necessary modules for the implementation of the algorithm. The micro-controller pinout and connections are shown in the full hardware schematic in Fig.4.34. Two channels of the Analog-to-digital (A/D) module are used to read the module's voltage and current. The resolution of the A/D module is 10-bits, and the A/D conversion time is $19.72\mu s$. The A/D time is relatively small compared to the sampling frequency of the algorithm which is 10 KHz .

The MPPT unit uses the Digital Pulse Width Modulation (DPWM) module to directly control the duty-cycle of the DC-DC converter. The DPWM module can produce up to a 10-bit resolution output. The choice of the DPWM setting is very critical since the switching frequency f_s and the resolution bits are inversely proportional. The resolution bits formula, which is found in the micro-controller datasheet, is

$$\text{Resolution} = \frac{\log\left(\frac{F_{\text{osc}}}{F_{\text{PWM}}}\right)}{\log(2)}, \quad (4.8)$$

where, F_{osc} is the frequency of the micro-controller clock, and F_{PWM} is the frequency of the PWM output. A large switching frequency is imperative to reduce the switching losses in the buck converter, while more DPWM resolution bits are essential to control the duty-cycle in small steps. The setting that was used for the hardware prototype are a PWM frequency of 98.039KHz which leads to a resolution of 7-bits. Consequently, the smallest step-size that can be achieved is $1/2^7$ (*i.e.* 0.0078).

The built-in Interrupt Service Routine (ISR) function is used to enable the partial shading periodic interrupts. An LCD and a keypad were added to the system to enable the interface between the MPPT unit and the user. The keypad allows the user to choose which algorithm to algorithm to run, and the LCD displays the status of the running algorithm. Finally, the Universal Asynchronous Receiver/Transmitter (UART) is used as a medium of communication between the microcontroller and the computer to record input/output data. This communication is accomplished via a serial DB9 cable.

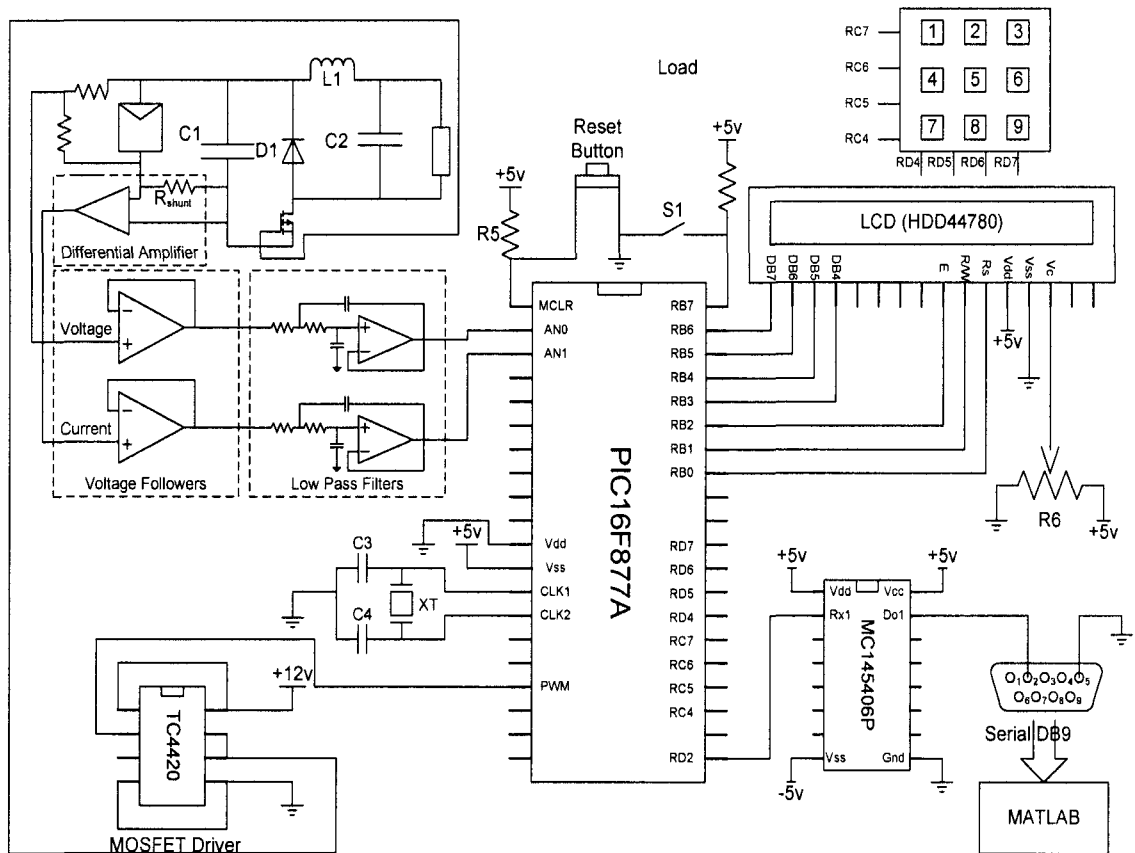


Figure 4.34 Full hardware schematic with the microcontroller and the interface

4.6. Experimental Results

The experimental process was done using artificial lights, which produced around $6.5W$ from the selected PV panel. There are some limitations in the experimental procedure, such as controlling the insolation level, or creating user-defined insolation schemes. Thus, the experimental results were not as diversified as the simulation results. However, the experimental setup allowed us to test the functionality of the proposed algorithm on commercial microcontrollers. Moreover, a conventional algorithm was also implemented using the same experimental setup for comparison with the proposed algorithm. As mentioned earlier, the results were recorded using the DB9 serial communication between the electrical circuit and the computer. The output voltage $V_{pv}[k]$ and the output current $I_{pv}[k]$ were recorded periodically over 500 samples and the output power $P_o[k]$ was calculated using $P_o[k] = V_{pv}[k] * I_{pv}[k]$.

In this section we present, experimental results of the proposed algorithm response, experimental results of an adaptive P&O algorithm, and finally a comparison and discussion between the two responses.

For the proposed algorithm, the module's output voltage $V_{pv}[k]$ is shown in Fig.4.35, and its output current $I_{pv}[k]$ is shown in Fig.4.36. The output voltage starts dropping from around $20V$ till it reaches the maximum power voltage V_{mp} (*approx.* $17.5V$). Similarly, the output current starts rising from $0A$ till it reaches the maximum power current I_{mp} (*approx.* $370mA$).

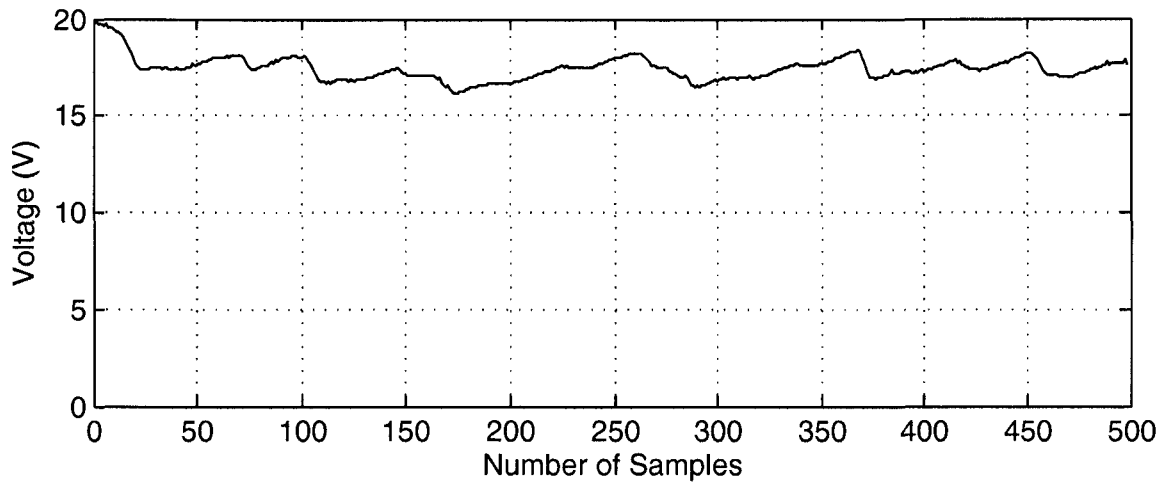


Figure 4.35 Experimental output voltage of the proposed algorithm

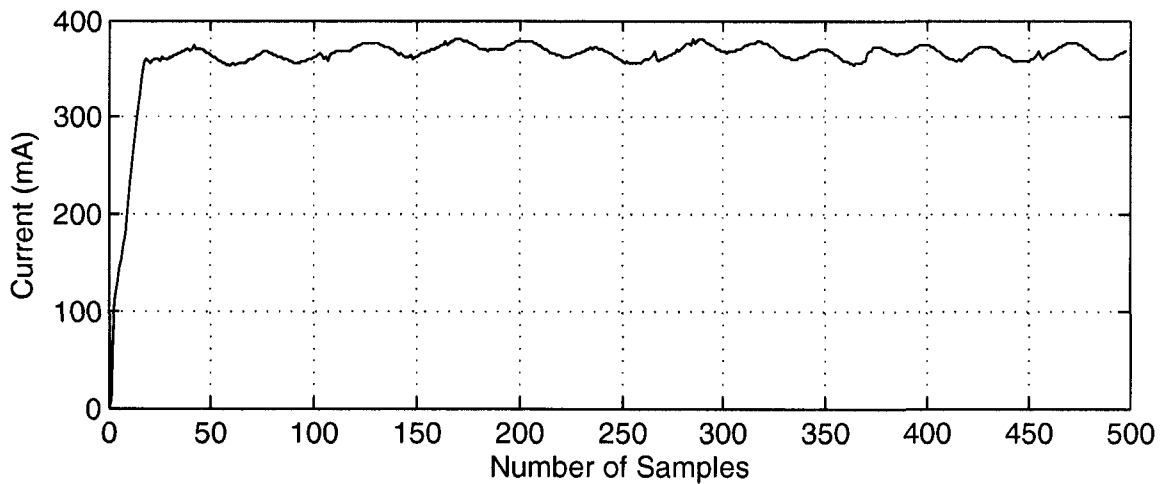


Figure 4.36 Experimental output current of the proposed algorithm

The module's output power $P_o[k]$, is shown in Fig.4.37. As can be seen the maximum power P_m (approx. $6.5W$) is achieved after 18 samples. This maximum power corresponds to the maximum power voltage and the maximum power current (*i.e.* $P_m[k] = I_{mp}[k] * V_{mp}[k]$).

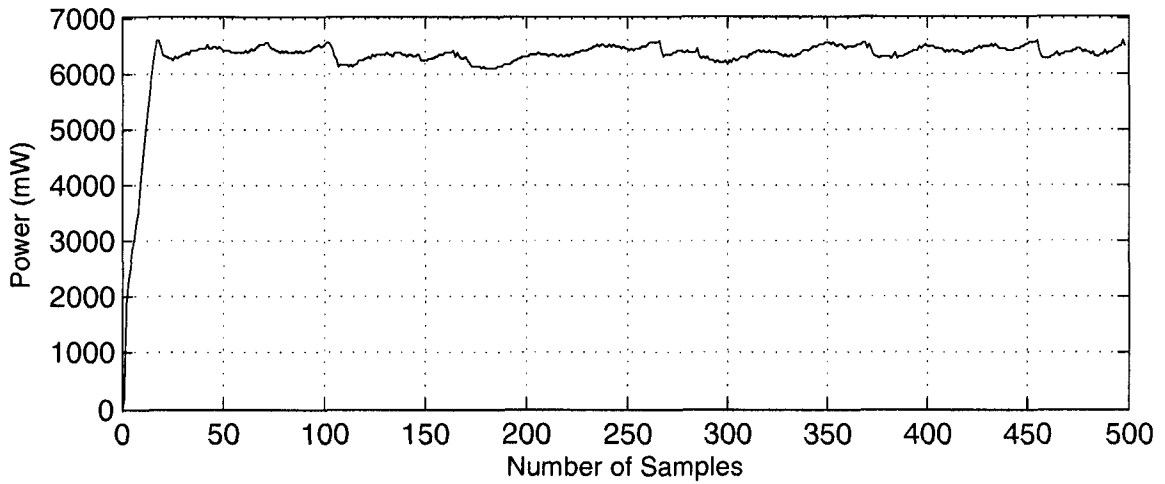


Figure 4.37 Experimental output power of the proposed algorithm

4.6.1 Comparison with adaptive P&O

An adaptive P&O algorithm is loaded into the microcontroller, and the results are presented in Fig. 4.38-4.40. The output voltage resulted from the adaptive P&O is shown in Fig.4.38, the voltage drops till it reaches the maximum power voltage V_{mp} (approx. 17.5V), and the output current, shown in Fig.3.39, rises till it reaches the maximum power current (approx. 350mA). The resulting output power is shown in Fig.4.40.

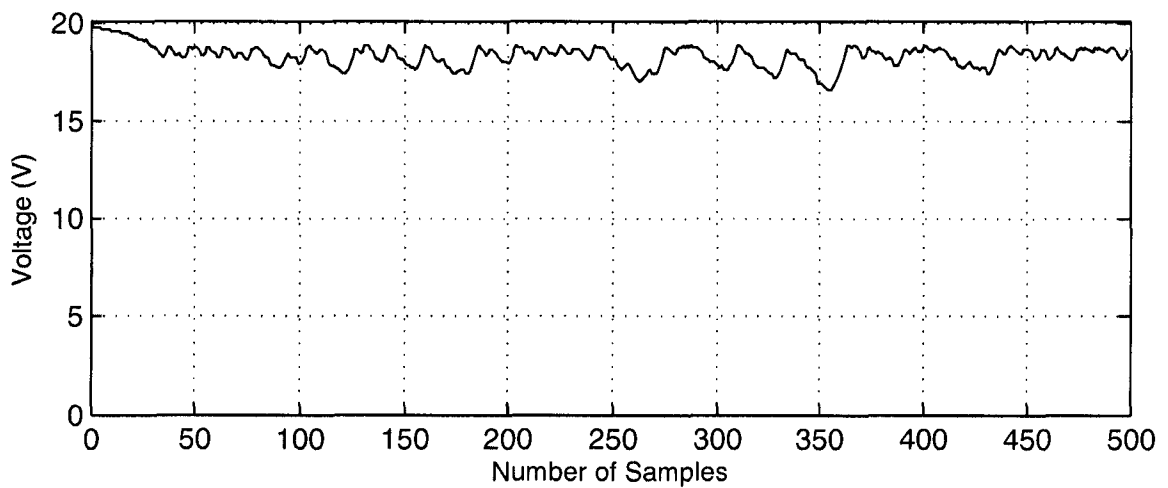


Figure 4.38 Experimental output voltage of an adaptive P&O

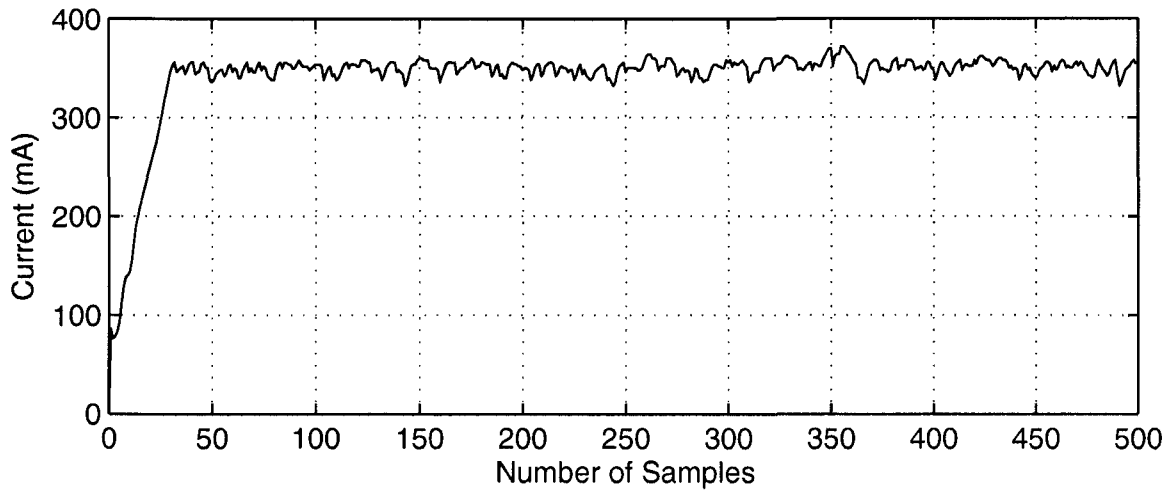


Figure 4.39 Experimental current voltage of an adaptive P&O

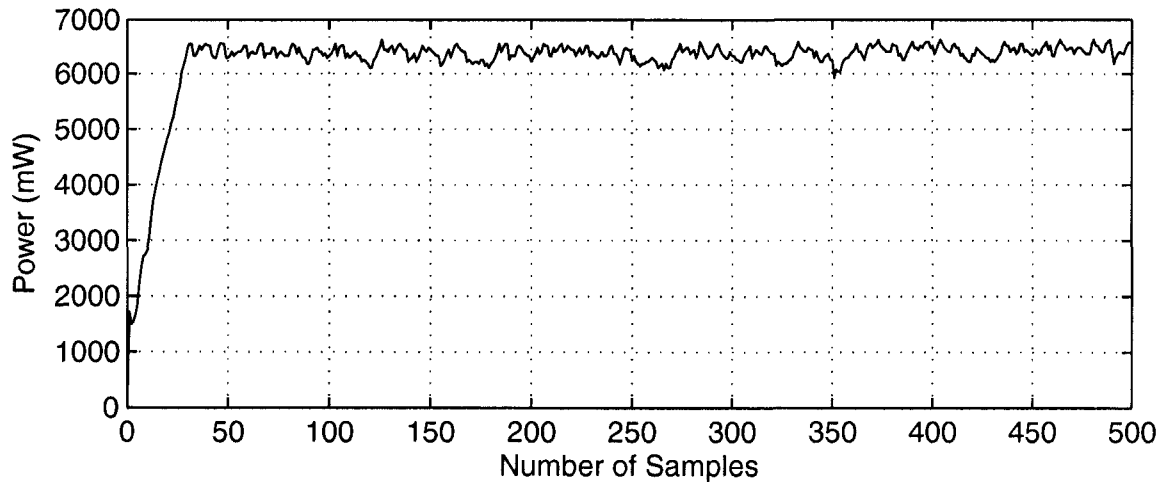


Figure 4.40 Experimental output power of an adaptive P&O

The responses of both algorithms are shown in Fig.4.41. As can be seen, the proposed algorithm has a relatively better transient response, which is due to the introduction of the proposed adaptive step-size. The error between the ideal response and the responses of the two algorithms (*i.e.* proposed and adaptive P&O) is shown Fig.4.42. The average of the error function due to the adaptive P&O response was calculated to be

9.0936e4. The average of the error function due to the proposed algorithm response was calculated to be 5.7883e4; this corresponds to an efficiency improvement of 5.53%.

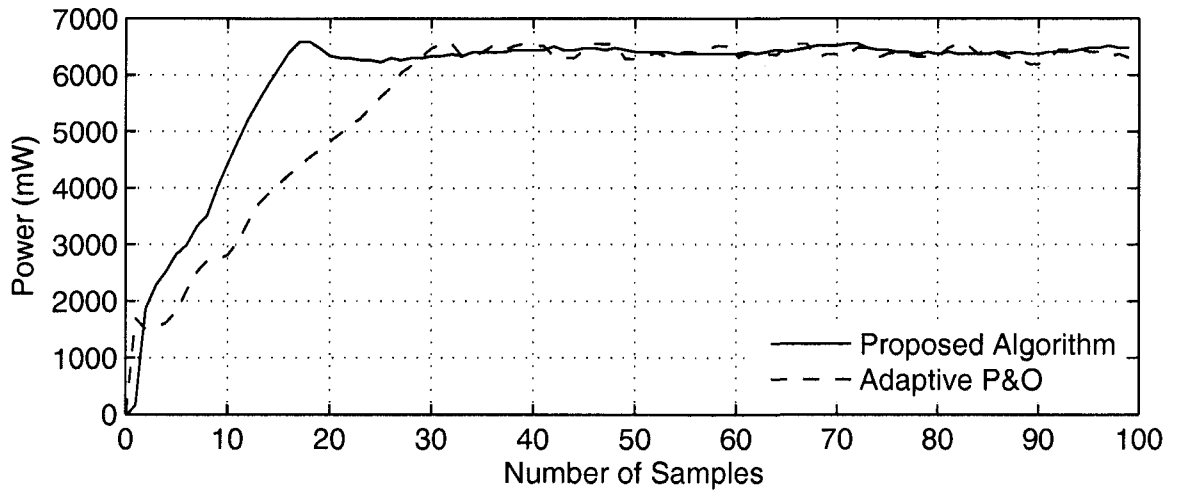


Figure 4.41 Comparison between the proposed algorithm and an adaptive P&O

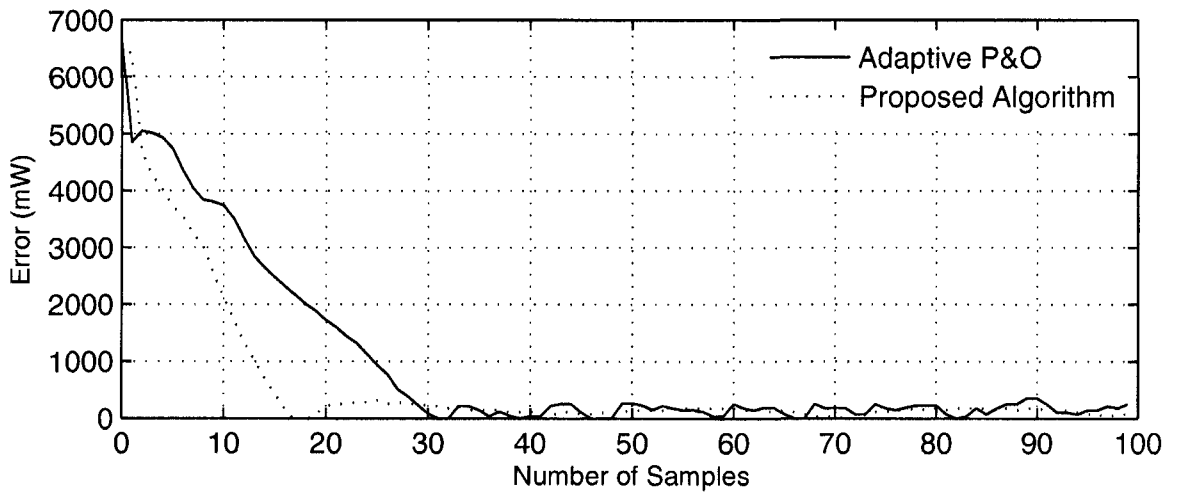


Figure 4.42 Error comparison between the proposed algorithm and an adaptive P&O

4.7. Conclusion

In this chapter, simulation and experimental results of the proposed algorithm have been presented. The simulations were run in SIMULINK environment, where the response of the proposed algorithm has been analyzed under several irradiation schemes. The results have been compared to the responses of several conventional algorithms, showing the improvements in transient, dynamic, and steady-state responses. An experimental setup has also been presented utilizing a micro-controller and a buck converter. Simulation results have been presented showing an improvement in the transient response over an adaptive P&O algorithm.

Chapter 5. Conclusions

5.1. Summary

In this work, a new algorithm has been proposed for improving the maximum power point tracking in PV systems. A modified rule for updating the reference variable, *i.e.* current/voltage or duty-cycle, has been presented. The algorithm incorporates new schemes for overcoming the challenges associated with rapidly changing insolation levels and the effect of partial shading.

An introduction to PV panels and their electrical characteristics has been presented in chapter 1. Specifically, the output power P_o of PV modules was analyzed with respect to their output voltage V_{pv} and output current I_{pv} . Starting from these characteristics, the importance of maximum power point tracking (MPPT) units has been shown. This was followed by addressing the common issues that most MPPT algorithms suffer from.

Several existing MPPT algorithms which include (P&O, ICM, and open-circuit voltage/short circuit current, etc) have been discussed in chapter 2. Moreover, some

selected works on MPPT algorithms has been discussed, which cover the main improvements done in this field.

A more efficient algorithm been proposed in chapter 3 for improving the maximum power point tracking in PV systems. The proposed algorithm has incorporated techniques to overcome the challenges of rapidly changing atmospheric conditions and partial shadings. Moreover, the algorithm has been designed to be suitable for implementation on commercial microcontrollers. A modified rule for updating the control variable (duty-cycle) has been presented. Such an approach can locate the operating point more precisely; thereby leading to an accurate step-size update. At rapidly changing atmospheric conditions, large power fluctuations (dP_2) occur within the sampling period which can mislead the tracking process. This issue has been addressed by introducing a new technique for the separation of the total power change (dP) into components dP_1 and dP_2 . After calculating dP_1 and dP_2 , the algorithm is able to calculate the correct tracking direction by comparing these power components. Finally, the issue of partial shading (multiple peaks in the power function) has also been taken into consideration by the proposed algorithm. The constant relation, *i.e.* $\alpha = I_{mp} / P_m$ is exploited, where P_m and I_{mp} denote maximum power and corresponding maximum power current respectively was exploited to. Based on this relation, periodic interrupt routines are invoked to estimate the expected global maximum power P_m of the present operating current I_{pv} using ($P_m = \alpha I_{pv}$), which is then compared with the actual output power P_o to ensure that the module is operating at the global maximum.

The simulation and experimental results have been presented validating the performance and functionality of the proposed algorithm. The simulations have been

done using SIMULINK where the different aspects of the model design and parameters have been detailed. The simulation results were divided into that of the transient/steady-state response, and the dynamic response. The first simulation environment was under fixed insolation levels ($1000W/m^2$). The output results of the proposed algorithm were compared to the output results of the P&O algorithm with different step-size values. The comparison figures were presented along with a table summarizing the efficiency improvement in both transient and steady-state responses. Second, a user-defined irradiation schemes were created to test the dynamic response of the algorithm, especially under rapidly changing atmospheric conditions. Two irradiation schemes have been created, one with fast descending insolation levels, and the second with a sudden insolation drop and fast ascending insolation levels. The output results of the first irradiation scheme were compared to the response of an adaptive P&O algorithm, while the output results of the second irradiation scheme were compared to the response of an adaptive ICM. The comparison figures and a table have been presented and discussed showing the improvement in the dynamic response. Finally, a hardware prototype have been discussed and implemented, the components and parameters related to the hardware design have been analyzed. The hardware prototype has been implemented using an 8-bits-architecture microcontroller, a buck DC-to-DC converter and an $85W$ PV panel. Artificial lights have been used for the experiment and the experimental results have been presented for the proposed algorithm and for an adaptive P&O algorithm. The results have been compared showing an improvement in the transient response.

5.2. Future Work

The presented MPPT algorithm was designed based on the characteristics of the buck dc-to-dc converter; hence, the adaptive step-size design could be altered for other converter topologies. Moreover, the algorithm could be updated to include more characteristics such as power regulations for battery charging applications, the ability to control single phase or three phase power systems (e.g. grid-connected or stand-alone systems).

Since artificial lights were being used for the experimental process, the experimental results were limited to the response of a fixed insolation level. The experimental results could be expanded using a PV array simulator (e.g. Agilent SAS B350). Such simulators allow creating an insolation profile, or simulating partial shading conditions.

The presented hardware prototype could be implemented on a printed circuit board (PCB) with the proposed algorithm loaded into the micro-controller. The overall unit can be developed as an end-user-product with different power specifications.

References

- [1] Renewable Energy Policy Network for the 21st Century, *Renewables 2007 Global Status Report*, REN21, Bali, Indonesia, 2007.
- [2] R. Messenger and J. Ventre, *Photovoltaic Systems Engineering*, 2nd ed., Boca Raton, Florida: CRC Press, 2004.
- [3] A. Luque and S. Hegedus, *Handbook of Photovoltaic Science and Engineering*, 1st ed., West Sussex, UK: Wiley, 2003.
- [4] M. R. Patel, *Wind and Solar Power Systems*, 1st ed., Boca Raton, London: CRC Press, 2003.
- [5] E. Koutroulis, K. Kalaitzakis, and N.C. Voulgaris, "Development of a microcontroller-based, photovoltaic maximum power point tracking control system," *IEEE Trans. Industrial Electronics*, vol. 53, pp. 46-54, 2001.
- [6] J. Youngseok, S. Junghun, Y. Gwonjong, and C. Jaeho, "Improved perturbation and observation method (IP&O) of MPPT control for photovoltaic power systems," *Proc. IEEE Photovoltaic Specialists Conf.*, pp. 1788-1791, 2005.
- [7] J. H. Park, J. Y. Ahn, B. H. Cho, and G. J. Yu, "Dual-module-based maximum power point tracking control of photovoltaic systems," *IEEE Trans. Industrial Electronics*, vol. 53, no. 4, pp. 1036-1047, 2006.
- [8] J. H. Lee, H. Bae, and B.H. Cho, "Advanced incremental conductance MPPT algorithm with a variable step size," *Proc. IEEE Power Electronics and Motion Control Conf.*, pp. 603-607, 2006.
- [9] N. S. D'Souza, L. A. C. Lopes, and X. J. Liu, "An intelligent maximum power point tracker using peak current control," *IEEE Power Electronic Specialists PESC Conf.*, pp. 172-177, 2005.
- [10] N. Mutoh, M. Ohno, and T. Inoue, "A method for MPPT control while searching for parameters corresponding to weather conditions for PV generation systems," *IEEE Trans. Industrial Electronics*, vol. 53, no. 4, pp. 1055-1065, 2006.
- [11] C. W. Tan, T. C. Green, and C. A. H. Aramburo, "A current-mode controlled maximum power point tracking converter for building integrated photovoltaics," *European Power Electronics and Applications Conf.*, pp. 1-10, 2007.
- [12] N. Femia, G. Petrone, G. Spagnuolo, and M. Vitelli, "Optimization of perturb and observe maximum power point tracking method," *IEEE Trans. Power Electronics*, vol. 20, no. 4, pp. 963-973, 2005.

- [13] A. Zbeeb, V. Devabhaktuni, A. Sebak, and L. Maheshwari, "A new microcontroller-based MPPT algorithm for photovoltaic applications," *Proc. Energy and Environment International Conf.*, vol. 40, pp. 832-835, 2009. **(Awarded best student paper)**
- [14] R. Leyva, C. Alonso, L. Queinnec, A. C. Pastor, D. Lagrange, and L. Martinez-Salamero, "MPPT of photovoltaic systems using extremum-seeking control," *IEEE Trans. Aerospace and Electronic Systems*, vol. 42, pp. 249-258, 2006.
- [15] Z. Yan, L. Fei, Y. Jinjun, and D. Shanxu, "Study on realizing MPPT by improved incremental conductance method with variable step-size," *IEEE Industrial and Electronics Applications Conf.*, pp. 547-550, 2008.
- [16] D. Lee, H. Noh, D. Hyun, and I. Choy, "An improved MPPT converter using current compensation method for small scaled PV-Applications," *IEEE Applied Power Electronics Conf. and Exposition*, vol. 1, pp. 540-545, 2003.
- [17] N. D'Souza, N. Lopez, and X. Liu, "Peak current control based maximum power point trackers for faster transient responses," *IEEE Canadian Conf. on Electrical and Computer Eng. Canadian Conf., CCECE*, pp. 659-663, 2006.
- [18] C. Won, D. Kim, S. Kim, W. Kim, and H. Kim, "A new maximum power point tracker of photovoltaic arrays using fuzzy controller," *IEEE Power Electronics Specialists Conf.*, vol. 1, pp. 396-403, 1994.
- [19] J. Ko, B. Jung, K. Park, C. Choi, and D. Chung, "Maximum power point tracking control of PV system for DC motors drive with neural networks," *IEEE Smart Manufacturing Application International Conf.*, pp. 514-519, 2008.
- [20] K. Samangkool and S. Premrudeepreechacharn, "Maximum power point tracking using neural networks for grid-connected photovoltaic system," *IEEE Future Power Systems International Conf.*, pp. 1-4, 2005.
- [21] W. Xiao and W. G. Dunford, "A modified adaptive hill climbing MPPT method for photovoltaic power systems," *IEEE Power Electronics Specialists Conf.*, pp. 1957-1963, 2004.
- [22] J. H. Lee, H. S. Bae, S. H. Park, and B. H. Cho, "Constant resistance control of solar array regulator using average current mode control," *IEEE Applied Power Electronics Conf.*, pp. 1544-1549, 2006.
- [23] F. Liu, S. Duan, F. Liu, B. Liu, and Y. Kang, "A variable step size INC MPPT method for PV systems," *IEEE Trans. Industrial Electronics*, vol. 55, no. 7, pp. 2622-2628, 2008.
- [24] J. H. Lee, H. Bae, and B. H. Cho, "Advanced incremental conductance MPPT algorithm with a variable step size," *IEEE Power Electronics and Motion Control, EPE-PEMC Conf.*, pp. 603-607, 2006.

- [25] D. Stone, M. Foster, C. Bingham, and P. Stewart, "Digitally controlled converter with an adaptive step-size for maximum power point tracking for photovoltaic applications," *IEEE Industrial Electronics Conf.*, pp. 703-706, 2008.
- [26] D. Sera, T. Kerekes, R. Teodorescu, and F. Blaabjerg, "Improved MPPT method for rapidly changing environmental conditions," *Proc. IEEE Int. Symp. Industrial Electronics*, pp. 1420-1425, 2006.
- [27] K. H. Hussein, I. Muta, T. Hoshino, and M. Osakada, "Maximum photovoltaic power tracking: an algorithm for rapidly changing atmospheric conditions," *IEEE Proc. Gener. Transm. Distrib.*, vol. 142, no. 1, pp. 59-64, 1995.
- [28] W. Wenkai, N. Pongratananukul, Q. Weihong, K. Rustom, T. Kasparis, and I. Batarseh, "DSP-based multiple peak power tracking for expandable power system," *IEEE Applied Power Electronics Conf. and Exposition*, vol. 1, pp. 525-530, 2003.
- [29] K. Kobayashi, I. Takano, and Y. Sawada, "A study on a two stage maximum power point tracking control of a photovoltaic system under partially shaded insolation conditions," *IEEE Power Engineering Society General Meeting*, p. 2617, 2003.
- [30] N. Mutoh, M. Ohno, and T. Inoue, "A Method for MPPT control while searching for parameters corresponding to weather conditions for PV generation systems," *IEEE Trans. Industrial Electronics*, vol. 53, no. 4, pp. 1055-1065, 2006.
- [31] N. Mohan, T. M. Undeland, and W. P. Robbins, *Power Electronics: Converters, Applications, and Design*, 3rd ed., Wiley, 2002.
- [32] W. K. Chen, *The Circuits and Filters Handbook*, 2nd ed., CRC Press, 2003.
- [33] A. Zbeeb, V. Devabhaktuni, and A. Sebak, "Improved photovoltaic MPPT algorithm adapted for unstable atmospheric conditions and partial shading," *IEEE International Conference on Clean Energy*, Accepted, Capri, Italy, 2009.

Appendix. MATLAB Codes

Matlab Code for plotting the I - V , P - V , and P - I characteristics

```
Ns = 36;      %Number of cells in series
Np = 1;      %Number of cells in parallel

q = 1.60e-19;    %charge of an electron
K = 1.38e-23;    %Boltzman's constant
A = 1.09;        %Ideality factor

T = 25 + 273;    %Temperature (Kelvin)

Tr = 25 + 273;   %Reference temperature

Isc = 5.46;      %Short-circuit current
                %at standard conditions
Ki = 2.2e-3;     %Short-circuit current
                %tempeature coefficient
S = 1000;       %Insolations

Rs = 0.141;
Rsh = 1000;

Irr = 2.54e-09;  %Saturation current
Ego = 1.13;

Irs = Irr*(T/Tr)^3 * exp( (q*Ego/(K*A)) * (1/Tr-1/T) );
                %Calculation of saturation current

Iph = ( Isc + Ki*(T-Tr) ) * (S)/1000;
                %Calculation of photon-generated
                %current

Voc = (1 / (q / (Ns * A * K * T))) * log(Iph / Irs);
Vo = 0:0.001:Voc;    %Calcualte open-circuit voltage

Io = Np * Iph - Np * Irs * ( exp(q*(Vo)/(Ns*A*K*T)) - 1 );
Io = Io - ( Io .* Rs) ./ Rsh;    %Shunt Resistance
Io = Io - Np * Irs .* ( exp(q.*Io.*Rs/(Ns*A*K*T)) - 1 );
                %Series Resistance

P = (Io .* Vo)./30;
                %Calculation of output power

plot(Vo, Io)
hold
plot(Vo, P)
%plot(Io, P)
xlabel('Module Voltage (V)');
ylabel('Module Current (A)');
%axis([0 30 0 6])
```

Matlab Code for plotting the relationship between P_m and I_{mp}

```

Ns = 36;
Np = 1;

q = 1.60e-19;
K = 1.38e-23;
A = 1.092;
%T = 25 + 273;

Tr = 25 + 273;

Isc = 5.34;
Ki = 2.12e-3;
%S = 1000;

Irr = 2.54e-09;
Ego = 1.13;

Smin = 100;
Tmin = 10 + 273;
Smax = 1000;
Tmax = 50 + 273;

R = ones(Tmax-Tmin+1, Smax-Smin+1);

for S = Smin:Smax
    for T = Tmin:Tmax

        Irs = Irr*(T/Tr)^3 * exp( (q*Ego/(K*A)) * (1/Tr-1/T) );

        Iph = ( Isc + Ki*(T-Tr) ) * (S+300)/1000;

        Voc = (1 / (q / (Ns * A * K * T))) * log(Iph / Irs);
        Vo = 0:0.01:Voc;

        Io = Np * Iph - Np * Irs * ( exp(q*Vo/(Ns*A*K*T)) - 1 );

        P = Io .* Vo;

        mp = max(P);

        for i = 1:length(P)
            if (P(i) == mp)
                break
            end
        end

        R(T-Tmin+1,S-Smin+1) = (Io(i)) ./ mp;

    end
end
end

```

```

T = ones(Tmax-Tmin+1, Smax-Smin+1);
S = ones(Tmax-Tmin+1, Smax-Smin+1);

for i = Tmin:Tmax
    for j = Smin:Smax
        T(i-Tmin+1, j-Smin+1) = j;
    end
end

for i = Tmin:Tmax
    for j = Smin:Smax
        S(i-Tmin+1, j-Smin+1) = i-273;
    end
end

surf(T, S, R)

xlabel('Irradiation');
ylabel('Temperature');
zlabel('Vmp/Voc');
title('Maximum Power Current / Maximum Power Ratio');

```

Matlab Code for plotting dP/dV

```
Ns = 36;
Np = 1;

q = 1.60e-19;
K = 1.38e-23;
A = 1.092;
T = 80 + 273;

Tr = 25 + 273;

Isc = 5.34;
Ki = 2.12e-3;
S = 1000;

Irr = 2.54e-09;
Ego = 1.13;

Irs = Irr*(T/Tr)^3 * exp( (q*Ego/(K*A)) * (1/Tr-1/T) );

Iph = ( Isc + Ki*(T-Tr) ) * (S)/1000;

Voc = (1 / (q / (Ns * A * K * T))) * log(Iph / Irs);
Vo = 0:0.01:Voc;

Io = Np * Iph - Np * Irs * ( exp(q*Vo/(Ns*A*K*T)) - 1 );

P = Io .* Vo;

dp = diff(P,1);
t = 0:Voc/length(dp):Voc-Voc/length(dp);
plot(t,abs(dp))
hold
plot(Vo, P/100)
xlabel('Cell Voltage (V)');
ylabel('Cell Power (W)');
title('Solar Cell P-V Characteristic');
hold
```

Matlab Code for the P&O algorithm (SIMULINK)

```
% Initialize MPPT
%
global Dref;
global Dold;
global Increment;
global Pold;
global DeltaI;

Pold = 0;
Dref = 0.1;
Dold = 0;
Increment = 1;
DeltaI = 0.015;

function y = MPPT(u)

global Pold;
global Dref;
global Dold;
global Increment;
global DeltaI;

DrefH = 0.99;
DrefL = 0;

P = u(1) * u(2);

if (P < Pold)
    Increment = -Increment;
end

Dref = Dref + Increment*DeltaI;
%

if (a < 0.0005)
    DeltaI = DeltaI_Old - 0.0005;
end
if (a > 0.0005)
    DeltaI = DeltaI_Old + 0.001;
end

if(DeltaI > 0.01)
```

```
    DeltaI = 0.01;
end

if (DeltaI < 0.002)
    DeltaI = 0.002;
end

if (Dref > DrefH)
    Dref = DrefH;
end

if (Dref < DrefL)
    Dref = DrefL;
end

y(3) = (P - Pold) / (Dref - Dold);
y(4) = DeltaI;

Pold = P;
Dold = Dref;

y(1) = P;
y(2) = DeltaI;
y(3) = DeltaI;
y(4) = Dref;
y(5) = P;
```